Spacecraft Attitude Estimation based on Temperature Measurements in Cuboid Configuration

Tobias Posielek, Johann Reger

In any spacecraft mission it is vital to have knowledge about the attitude. In this context, multiple ways can be employed to estimate the current attitude of the spacecraft. As temperature sensors are cheap and lightweight they appear to be a viable alternative. A method is investigated to estimate the attitude of a spacecraft based on twelve temperature sensors in a cuboid configuration. The method relies on a proposed mathematical model governing the temperature and attitude dynamics and employs non-linear observer design. Further, it is investigated if the attitude estimation is still possible if some of the sensors are malfunctioning. The proposed algorithms are validated using real mission data.

Spacecraft Attitude Estimation based on Temperature Measurements in Cuboid Configuration

Tobias Posielek[a,*], Johann Reger[b]

[a] *Institute of System Dynamics and Control, German Aerospace Center (DLR), Muenchner Str. 20, D-82234 Wessling, Germany, tobias.posielek@dlr.de*

[b] *Control Engineering Group, Technische Universität Ilmenau, P.O. Box 10 05 65, D-98684, Ilmenau, Germany, johann.reger@tu-ilmenau.de*

Abstract

In any spacecraft mission it is vital to have knowledge about the attitude. In this context, multiple ways can be employed to estimate the current attitude of the spacecraft. As temperature sensors are cheap and lightweight they appear to be a viable alternative. A method is investigated to estimate the attitude of a spacecraft based on twelve temperature sensors in a cuboid configuration. The method relies on a proposed mathematical model governing the temperature and attitude dynamics and employs non-linear observer design. Further, it is investigated if the attitude estimation is still possible if some of the sensors are malfunctioning. The proposed algorithms are validated using real mission data.

1. Introduction

Temperature sensors are commonly employed on every spacecraft mission. They allow monitoring the temperature of individual electrical components and enable to take measures if any of these components exceed their temperature limits. Consequently, they allow the identification of heat sources or their absences which can be used for a multitude of purposes. One of them has found more and more interest in research within the last few years, namely the attitude estimation of the spacecraft based on temperature measurements.

There are multiple scenarios in which the application of attitude estimation based on temperature data can be beneficial. Three of them being safe mode operation, low cost satellites and sensor failure. In most conventional operation modes, the most precise attitude of the spacecraft is obtained using star trackers as they give the highest accuracy. Adversely, its computational effort and costs are high. Furthermore, for every mission there exists a safe mode for the spacecraft. This mode may occur if any operating condition or events occur that may lead to loss of control of the spacecraft. It is usually designed in order to guarantee thermal and power survival of the spacecraft and their electrical components. Consequently, this mode focuses on detumbling, ensuring that the solar panels see enough sunlight and not letting any of the electrical components overheat. Therefore, non-essential and power consuming electrical components such as star trackers are usually turned off and the desired pointing accuracies are often not more than 10 degrees Herman et al. (2004). With the temperature sensors being cheap and having a low power consumption, the method proposed in this work is designated to be applied in this scenario to estimate the attitude. Additionally, the temperature measurements and their resulting estimates can also be combined with other low cost measurements such as magnetometer or acceleration measurements. For the same reasons, it is clear, that the proposed method can also be applied for low cost satellites. Furthermore, spacecraft need fall back options in case their nominal attitude sensors fail. Temperature sensors are extremely cheap such that a multitude of them can be used in a hot redundant manner. This makes this method a reliable fall back option if for example the usually used star trackers fail. For all three applications discussed, it is important to note that the altitude of the considered orbits must not be too high, as for higher altitudes the influence of infrared and albedo irradiation is insignificant. For low earth orbits the proposed methods are applicable.

The attitude estimation is achieved by considering temperature sensors at the outside of the spacecraft which are mostly isolated from internal heat flows. Consequently, the temperature evolution is only governed by irradiations from Earth, Sun and deep space. Dependent on the amount of sensors and their configuration this allows an estimate of Sun and Earth position with respect to the spacecraft and consequently an estimate of the spacecraft's orientation with respect to an inertial frame. This estimate can be combined with other vector measurements from e.g. star trackers, sun sensors, Earth sensors, gyroscopes and GNSS to refine the attitude estimation Sidi (1997); Martin et al. (2004).

In a similar fashion, temperature data is used for orbit determination as proposed in Gourabi et al. (2019). Hereby, mainly the irradiations emitted by Earth are used

*Corresponding author.

in an unscented Kalman Filter design to estimate position and velocity of the spacecraft. In the follow-up work Gourabi et al. (2020), the albedo factor is simultaneously estimated as it usually varies significantly with the local terrain and cloud coverage.

While the underlying idea of attitude reconstruction based on temperature data is similar, the specific algorithm depends on the number of sensors used and their configuration.

The usage of only a single sensor is investigated in Posielek (2022) and Posielek and Reger (2022). This single sensor is already sufficient to estimate the attitude but only in a local instead of a global manner and its estimation algorithm requires at least three times the differentiation of the temperature signal which is difficult to fulfil for a signal in practice which is subject to noise.

Thus, it is desired that the temperature signal must be differentiated at most once. In order to achieve this, there must be at least three temperature sensors. This is investigated in Khaniki and Karimian (2014) for sensors orthogonal to each other. The resulting non-linear system of equations can be solved by an optimisation algorithm. However, because each sensor is influenced by the superposition of irradiation from Earth and Sun, the solution is not unique. The authors of Khaniki and Karimian (2014) propose the usage of an additional sensors pointing in opposite direction to the already existing ones to solve this ambiguity.

Instead of explicitly solving the non-linear system of equations, Labibian et al. (2017) proposes the usage of an unscented and extended Kalman filter to estimate the attitude. This extended Kalman filter is experimentally validated in a vacuum chamber equipped with a Sun simulator Labibian et al. (2016). The resulting accuracy is in the range of $0.2°$. Naturally, these errors are expected to be higher under non-laboratory conditions.

Despite this success with already three sensors, the advantages using twelve temperature sensors in a specific configuration are significant. The twelve sensors are divided into six pairs where each pair points into the direction of another positive or negative unit vector which is referred to as cuboid configuration. Every pair consists of two sensors with different visual absorption and emittance. This ensures that for a spacecraft which is not in solar eclipse, there are at least three sensor pairs that are under the influence of solar irradiation at all times. Additionally, the sensor pairs allow the estimation of the irradiation from Earth and Sun individually and not only their superposition as mentioned in Khaniki and Karimian (2014). These sensors in this configuration are commonly employed in industry and referred to as Coarse Earth Sun Sensors (CESS) Kramer (2002). They are used for example in safe mode to give rough estimations of the attitude Levenhagen et al. (2007).

In this work, a novel observer design is proposed for the introduced configuration and a proof of its convergence is given. This design has not been considered in literature before and is extremely transparent and simple to implement. It only consists of a linear differentiator and a non-linear transformation. No convergence of an optimisation method or of non-linear ordinary differential equations has to be shown. Additionally, the scenario of sensor outages is investigated, i.e. failure cases where some of the considered sensors do not provide reliable information any more. It can be shown that in most configurations with sensor outage, the proposed design can be adapted to still yield accurate estimates of the attitude. Finally, the proposed observers are validated on data from a real spacecraft mission.

Furthermore, parts of the Sections 5 and 8 have been submitted within Posielek (2022). However, Section 7 is completely novel and has not been discussed in aforementioned thesis.

The rest of the work is structured as follows. Section 2 provides the required notation necessary for the problem formulation and the observer design. In Section 3 the non-linear models governing the temperature, attitude and orbit dynamics are given. A compact formulation of the problem is given in Section 4 while Section 5 shows the observer design. The adaptation of the observer for a sensor outage is discussed in Section 7. Finally, the proposed observers are validated against real mission data in Section 8.

2. Notation

Much of the notation in this work is based on Markley and Crassidis (2014) and Posielek and Reger (2021). By $\mathbb{R}_+$ all positive real numbers are denoted. The i-th unit vector of $\mathbb{R}^n$ is defined by e_i. The identity and zero matrix of dimension n for $n \in \mathbb{N}$ are denoted by I_n and 0_n. The subscript n is neglected when the dimension of the matrix is clear. For an $n \in \mathbb{N}$ dimensional vector $x \in \mathbb{R}^n$ the i-th component is denoted by x_i and the components x_i to x_j where $i < j \leq n$ and $i, j \in \mathbb{N}$ are denoted by $x_{i:j} = [x_i \ \dots \ x_j]$. For any matrices $A_i \in \mathbb{R}^{p\times m}$ where $n, p, m \in \mathbb{N}$ the block diagonal matrix with $A_1, \dots, A_n$ on the main diagonal is denoted by $\operatorname{diag}(A_1, A_2, \dots, A_n)$. For a matrix $A \in \mathbb{R}^{n\times m}$ with $n > m$ and full rank the Moore-Penrose inverse with $A^+ = (A^\top A)^{-1}A^\top$ is denoted A^+ . Most of the notations regarding attitudes are borrowed from Markley and Crassidis (2014). Let

$$\mathbb{S}_i = \{x \in \mathbb{R}^{i+1} \mid \|x\| = 1\}$$

be the i-th unit sphere with $\|\cdot\|$ the Euclidean norm. The special orthogonal group is denoted by $\mathcal{SO}_3$

$$\mathcal{SO}_3 = \{A \in \mathbb{R}^{3\times 3} \mid AA^\top = I,\ \det(A) = 1\}$$

which contains all rotation matrices. The cross product matrix and the matrix required for quaternion multiplication are defined as

$$[u\times] = \begin{bmatrix} 0 & -u_3 & u_2 \\ u_3 & 0 & -u_1 \\ -u_2 & u_1 & 0 \end{bmatrix}, \quad \Xi(q) = \begin{bmatrix} q_4 I_3 + [q_{1:3}\times] \\ -q_{1:3}^\top \end{bmatrix}$$

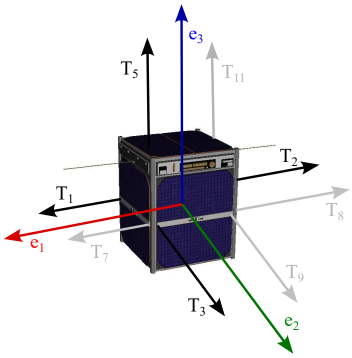

Figure 1: Configuration of the temperature sensors

for $u \in \mathbb{R}^3$ and $q \in \mathbb{S}_3$. In order to define the quaternion dynamics the matrix

$$\Omega(\omega) = \begin{bmatrix} -[\omega\times] & \omega \\ -\omega^\top & 0 \end{bmatrix}$$

for $\omega \in \mathbb{R}^3$ is introduced. With $A : \mathbb{S}^3 \to \mathcal{SO}_3$ the transformation from quaternion into rotation matrix is denoted which is defined by

$$A(q) = \|q\|^{-2}\Big((q_4^2 - \|q_{1:3}\|^2)I_3 + 2q_{1:3}q_{1:3}^\top - 2q_4[q_{1:3}\times]\Big)\,.$$

he inverse quaternion q^{-1}, the quaternion multiplication of $q, \bar{q} \in \mathbb{S}_3$ denoted by $\otimes$ and the error quaternion q^{e} are defined by

$$q^{-1} = [-q_{1:3}^\top, q_4]^\top\,, \quad q \otimes \bar{q} = \begin{bmatrix}\Xi(\bar{q}) & \bar{q}\end{bmatrix} q\,, \quad q^{\mathrm{e}} = q \otimes \bar{q}^{-1}\,.$$

The inverse of the sine and cosine with the image $[-\frac{\pi}{2}, \frac{\pi}{2}]$ and $[0, \pi]$ are written denoted by asin and acos, respectively. The operators $\wedge$ and $\vee$ denote logical conjunction and disjunction, respectively. The angle between two vectors $r, s \in \mathbb{R}^3$ and two quaternions $q, \bar{q} \in \mathbb{S}_3$ is defined as

$$\angle(r, s) := \operatorname{acos}\left(\frac{r^\top}{\|r\|}\frac{s}{\|s\|}\right) \quad \angle(q, \bar{q}) := 2\operatorname{acos}(q \otimes \bar{q}^{-1})\,.$$

3. Modelling

A rigid body spacecraft with twelve sensors pointing along the individual positive and negative body axes is considered. Along each axis there are two sensors with different physical parameters. One sensor of each pair has a surface which is reflective silver while the other one is black. These surfaces have different thermal coefficients $\alpha_{\mathrm{s},i}$ and $\varepsilon_{\mathrm{s},i}$. A temperature measurement of a black surface will be denoted by the superscript $\cdot^{\mathrm{B}}$ while one of a silver surface will be denoted by $\cdot^{\mathrm{S}}$. One sensor is located at each side of the spacecraft which is referred to as *cuboid configuration*, i.e. $n \in \{\pm e_1, \pm e_2, \pm e_3\}$ where n is the normal vector in body frame. A temperature measurement with the normal n is denoted with a subscript $\cdot_n$. In total

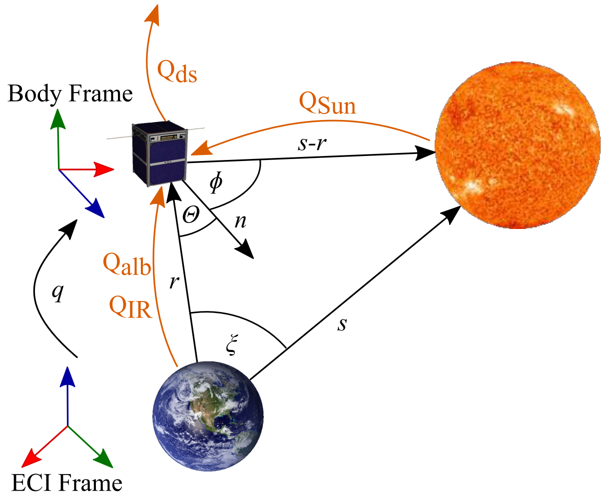

Figure 2: Illustration of the considered system. Courtesy: NASA)

there are twelve different temperature measurements T_n^i with $i \in \{\mathrm{B}, \mathrm{S}\}$ and $n \in \{\pm e_1, \pm e_2, \pm e_3\}$. The temperatures are arranged such that the first six temperatures are from black sensors and the second six from silver sensors, i.e. it is

$$T := [T_1, \ldots, T_{12}] := [T_{n_1}^{\mathrm{B}}, T_{n_2}^{\mathrm{B}}, \ldots, T_{n_6}^{\mathrm{B}}, T_{n_7}^{\mathrm{S}}, T_{n_8}^{\mathrm{S}}, \ldots, T_{n_{12}}^{\mathrm{S}}]$$

with the configuration $N^{\mathrm{con}} := \{n_1, n_2, \ldots, n_{12}\}$ and the normals $(n_1, n_2, \ldots, n_6) = (e_1, -e_1, e_2, -e_2, e_3, -e_3)$ and $(n_7, n_8, \ldots, n_{12}) = (n_1, n_2, \ldots, n_6)$. The configuration of these sensors is illustrated in Figure 1.

In order to describe the attitude quaternions $q \in \mathbb{S}_3$ are used which represent the attitude of the body frame of the spacecraft with respect to the Earth-centered inertial (ECI) frame. The parameters of the i-th temperature sensors shall be denoted by $c_i = [\alpha_{\mathrm{s},i}, C_i, Q_i^{\mathrm{d}}, A_{\mathrm{s},i}, \varepsilon_{\mathrm{s},i}]^\top$ where $\alpha_{\mathrm{s},i}$ is the solar absorptance, Q_i^{d} the dissipated power, C_i the thermal capacity, $A_{\mathrm{s},i}$ the surface area and $\varepsilon_{\mathrm{s},i}$ the emittance of the i-th temperature sensor. More details about these parameters can be found in Posielek (2018).

The overall system dynamics can be split into thermal, attitude and orbit dynamics.

3.1. Thermal Dynamics

An illustrative overview of the temperature dynamics can be seen in Figure 2. The model and notations of Posielek (2018) based on the work of Larson and Wertz (1991) and Meseguer et al. (2012) are used. The dynamics of the temperature are assumed to be governed solely by environmental heat. The dynamics have the form

$$\begin{aligned}\dot{T}_i = {} & Q_{\mathrm{sun}}(q, r, n_i, c_i) + Q_{\mathrm{alb}}(q, r, n_i, c_i) + Q_{\mathrm{IR}}(q, r, n_i, c_i) \\ & - Q_{\mathrm{ds}}(T_i, c_i) + Q_{\mathrm{dis}}(c) \end{aligned} \tag{1}$$

where Q_{sun} is the solar, Q_{alb} the albedo, Q_{IR} the infrared, Q_{ds} the deep space irradiation and Q_{dis} the dissipated heat and r the position of the spacecraft with respect to earth in ECI frame. Note that this is a simple model which assumes that the dissipative heat is constant and that neither conduction nor radiation exchange exists between different temperature nodes. The irradiations are defined as

$$Q_{\mathrm{sun}}(q,r,n_i,c_i) = \max\Big(\alpha(r,c_i)\cos(\phi(q,n_i)),0\Big) \tag{2}$$

$$Q_{\mathrm{alb}}(q,r,n_i,c_i) = \max\Big(\beta(r,c_i)F(\theta(q,r,n_i),r),0\Big) \tag{3}$$

$$Q_{\mathrm{IR}}(q,r,n_i,c_i) = \gamma(r,c_i)F(\theta(q,r,n_i),r) \tag{4}$$

$$Q_{\mathrm{ds}}(T_i,c_i) = \delta(c_i)T^4 \tag{5}$$

$$Q_{\mathrm{dis}}(c) = \frac{Q_i^{\mathrm{d}}}{C}\,. \tag{6}$$

They are introduced such that the attitude dependency is captured in the angles $\phi(q,n_i)$, $\theta(q,r,n_i)$ while the material and parameter dependencies are captured in the variables $\alpha(r,c_i)$, $\beta(r,c_i)$, $\gamma(r,c_i)$ and $\delta(c_i)$, respectively. These are defined by

$$\alpha(r,c_i) = \frac{1}{C_i}\alpha_{\mathrm{s},i}G_s(r)A_{\mathrm{s}}\nu(r) \tag{7a}$$

$$\beta(r,c_i) = \frac{1}{C_i}\rho_{\mathrm{alb}}(r)\alpha_{\mathrm{s},i}G_s(r)A_{\mathrm{s},i}\cos\big(\xi(r)\big) \tag{7b}$$

$$\gamma(r,c_i) = \frac{1}{C_i}\varepsilon_{\mathrm{e},i}A_{\mathrm{s},i}I_{\mathrm{IR}}(r),\;\; \delta(c_i) = \frac{1}{C_i}\varepsilon_{\mathrm{e},i}A_{\mathrm{s},i}\sigma_{\mathrm{s}} \tag{7c}$$

where $G_{\mathrm{s}}(r)$ is the solar constant dependent on the position and σ_{s} the Stefan-Boltzmann constant. The variables $\rho_{\mathrm{alb}}(r)$, $I_{\mathrm{IR}}(r)$ denote the albedo and infrared coefficient, respectively. These change significantly dependent on the terrain the satellite is passing. They are modelled as functions of latitude as in Peyrou-Lauga (2017). Note that α_i may be discontinuous due to the shadow function ν which models whether the satellite is in eclipse or sunlit i.e. $\nu = 0$ or $\nu = 1$, respectively. It is defined using a cylindrical shadow model with the Earth mean radius $r_\oplus$ and the position of the Sun s in ECI frame as

$$\nu(r) = \begin{cases} 0 & \text{if } r^\top \frac{s}{\|s\|} < 0 \wedge \|r - r^\top s\frac{s}{\|s\|^2}\| < r_\oplus \\ 1 & \text{otherwise} \end{cases}\,. \tag{8}$$

The angles $\phi(q,n_i)$, $\theta(q,r,n_i)$ and $\xi(r)$ influence the magnitude of the solar, albedo and infrared irradiation and are illustrated in Fig. 2. The angle $\theta(q,r,n_i)$ is the angle between the direction the i-th temperature sensor is pointing n_i and the spacecraft position r. The angle $\xi(r)$ is the solar zenith angle, which is the angle between spacecraft and Sun. The angle $\phi(q,n_i)$ denotes the angle between the direction the i-th temperature sensor is pointing n_i and the Sun $s-r$. Note that $s-r\approx s$ due to the norm of s being much larger than the norm of r. Thus, these angles amount to

$$\phi(q,n_i) = \mathrm{acos}\left(\frac{s^\top}{\|s\|}A(q)^\top n_i\right) \tag{9a}$$

$$\theta(q,r,n_i) = \mathrm{acos}\left(-\frac{r^\top}{\|r\|}A(q)^\top n_i\right) \tag{9b}$$

$$\xi(r) = \mathrm{acos}\left(\frac{r^\top}{\|r\|}\frac{s}{\|s\|}\right)\,. \tag{9c}$$

Note that r, s are given in ECI frame and n_i is given in body frame.

The form factor F is defined by

$$F(\theta,r) = \begin{cases} \frac{\cos(\theta)}{H^2} & \theta \le \frac{\pi}{2} - \mathrm{asin}\left(\frac{1}{H}\right) \\ F_{\mathrm{f},2} & \frac{\pi}{2} - \mathrm{asin}\left(\frac{1}{H}\right) < \theta < \theta_{\mathrm{crit}} \\ 0 & \theta \ge \theta_{\mathrm{crit}} \end{cases} \tag{10}$$

with $H = \frac{\|r\|}{r_\oplus}$ where $r_\oplus$ is the Earth mean radius, the critical angle $\theta_{\mathrm{crit}} = \frac{\pi}{2} + \mathrm{asin}\left(\frac{r_\oplus}{\|r\|}\right)$ and

$$\begin{aligned} F_{\mathrm{f},2} = {} & \frac{1}{2} - \frac{1}{\pi}\mathrm{asin}\left(\frac{\sqrt{H^2-1}}{H\sin(\theta)}\right) \\ & + \frac{1}{\pi H^2}\Big(\cos(\theta)\,\mathrm{acos}\big(-\sqrt{H^2-1}\cot(\theta)\big) \\ & - \sqrt{H^2-1}\sqrt{1-H^2\cos(\theta)^2}\Big)\,. \end{aligned}$$

3.2. Attitude Dynamics

The quaternion dynamics defining the angles $\phi(q,n_i)$ and $\theta(q,r,n_i)$ are described by

$$\dot{q} = \frac{1}{2}\Omega(\omega)q \tag{11}$$

where $\omega \in \mathbb{R}^3$ is the angular velocity of the spacecraft, the dynamics of which are described by Euler's rotation equation

$$\dot{\omega} = J^{-1}(-\omega \times J\omega) + J^{-1}u \tag{12}$$

with inertia matrix $J \in \mathbb{R}^{3\times 3}$ and control input $u \in \mathbb{R}^3$.

3.3. Orbit Dynamics

The orbit dynamics are commonly defined by a second order differential equation

$$\ddot{r} = f_r(r) \tag{13}$$

where f_r contains all forces acting on the spacecraft as discussed in e.g. Markley and Crassidis (2014). Note that the temperature dynamics are not very sensitive to errors in the estimation of r, because only the normalised vector $\frac{r}{\|r\|}$ is required for the calculation of the angles. Thus, for the upcoming analysis it is assumed that $r(t)$ is known either by the means of measurement or estimation based on (13).

This section is closed by introducing notations to render the problem statement more compact. Let the right-hand sides of the temperature dynamics be denoted by $f_T = Q_{\text{sun}} + Q_{\text{alb}} + Q_{\text{IR}} - Q_{\text{ds}} + Q_{\text{dis}}$, of the quaternion dynamics by $f_q(q,\omega) = \frac{1}{2}\Omega(\omega)q$, of Euler's rotation equation by $f_\omega(\omega) = J^{-1}(-\omega \times J\omega)$ and $g_\omega = J^{-1}$. The states are denoted by $x \in \mathbb{R}^{12}_{+} \times \mathbb{S}_3 \times \mathbb{R}^3$ with $x = (T_1, \dots, T_{12}, q^\top, \omega^\top)^\top$.

4. Problem Definition

The compact system resulting from the dynamics (1), (11) and (12) can be written as

$$\dot{T}_1 = f_T(T_1, q, r, n_1, c_1) \tag{14a}$$
$$\vdots \tag{14b}$$
$$\dot{T}_{12} = f_T(T_{12}, q, r, n_{12}, c_{12}) \tag{14c}$$
$$\dot{q} = f_q(q, \omega) \tag{14d}$$
$$\dot{\omega} = f_\omega(\omega) + g_\omega u \tag{14e}$$
$$y = h(x) \tag{14f}$$

with the output function $h : \mathbb{R}^{19} \to \mathbb{R}^{15}$

$$h(x) = \begin{bmatrix} T_1 & \dots & T_{12} & \omega \end{bmatrix}^\top .$$

The objective is to design an observer for the system (14) to estimate the attitude. An observer in the spirit of Besançon (2007) is defined by any system

$$\dot{\hat{X}} = F^{\text{obs}}(\hat{X}, u, y, t) \tag{15a}$$
$$\hat{x} = H^{\text{obs}}(\hat{X}, u, y, t) \tag{15b}$$

such that the estimate $\hat{x}$ is the real state x if the initial state is known, i.e. for all t holds $\hat{x}(t) = x(t)$ if $\hat{x}(0) = x(0)$. Additionally, the estimate $\hat{x}$ of an observer must converge to the real state x for any initial value, i.e. $\lim_{t\to\infty} \|x(t) - \hat{x}(t)\| = 0$.

For the proposed system this means in particular that the goal is to obtain an estimate of the attitude q based on the temperature measurements $T_1, \dots, T_{12}$.

5. Observer Design

An observer based on the first derivative of the temperature measurements and a non-linear transformation of the attitude is used. Figure 3 shows a block diagram which presents the idea of the algorithm proposed in the upcoming sections. First, a differentiator is designed to obtain an estimate of the filtered temperature as well as its derivative. These two signals of each sensor shall then be used in combination with their dynamics presented in Equations (14a) to (14c) to estimate the angles to Sun and Earth. These angles can be used to estimate the vectors of Sun and Earth in body coordinates. Finally, the actual desired attitude of the spacecraft can be estimated.

The angle estimation will be discussed in detail in the next sections. It turns out that this requires merely a linear inversion. The vector estimation consists of two parts. First, finding the measurements that contain useful information and second, using these measurements to estimate the vectors. These will turn out to be the result of multiple matrix multiplications. Finally, the real attitude estimation is a standard problem for which various different algorithms exist and will be discussed. The upcoming sections also answers the question of the system's observability by naturally solving the underlying inversion problem. Hereby for the remainder of this section it is assumed that the system is not in solar eclipse, i.e. there are at least six sensors on which solar irradiation is acting. The eclipse case is discussed in Section 6.2.

For brevity of exposition the arguments in the upcoming section are ommitted and a subindex $\cdot_i$ to denote the parameter vector is used, e.g. $\phi_i = \phi(q, n_i)$, $F_i = F(\theta(q, r, n_i), r)$ and $\alpha_i = \alpha(r, c_i)$.

5.1. Differentiator Design

The topic of differentiator design can be viewed as the observer design of a system which states are described by a chain of integrators. This fixed system structure facilitates the analysis and allows to show the convergence of a multitude of different observers such as linear, high gain or sliding mode differentiators Vasiljevic and Khalil (2006); Khalil (2002); Levant (2003); Levant et al. (2017), to name but a few. The prevalent problem for all observers is to find the right balance between performance and measurement noise rejection. The latter is achieved in an optimal manner for Gaussian white noise when a Kalman Filter is employed. For the proposed system class a first order differentiator for every temperature measurement is required to estimate the derivative. A simple high gain differentiator in the spirit of Khalil (2002) is proposed but any other differentiator should provide the desired estimates. Let $i \in \{1, \dots, 12\}$ be the index of the considered temperature measurement, then it is possible to use the following differentiator

$$\frac{\mathrm{d}}{\mathrm{d}t} \begin{bmatrix} \hat{T}_i \\ \dot{\hat{T}}_i \end{bmatrix} = \begin{bmatrix} 0 & 1 \\ 0 & 0 \end{bmatrix} \begin{bmatrix} \hat{T}_i \\ \dot{\hat{T}}_i \end{bmatrix} + \begin{bmatrix} \frac{a_1}{\varepsilon} \\ \frac{a_0}{\varepsilon^2} \end{bmatrix} (T_i - \hat{T}_i) \tag{16}$$

where a_0, a_1 are the coefficient that design the Hurwitz polynomial $a_0 + a_1 s + s^2$ and ε an additional design parameter. These parameters need to be chosen such that the bandwidth of the differentiator matches the bandwidth of the system and the magnitude of the measurement noise. For the considered orbits, the measurement noise is small compared to the sensitivity of the temperature with respect to the attitude. This allows combined with slow attitude dynamics to design the high gain observer appropriately to deal with the measurement noise. The proposed way in this work to obtain the differentiator parameters is by optimisation as carried out in Section 8.3.1. The estimated values $\dot{\hat{T}}_i$ and $\hat{T}_i$ are used in the following to estimate the angles.

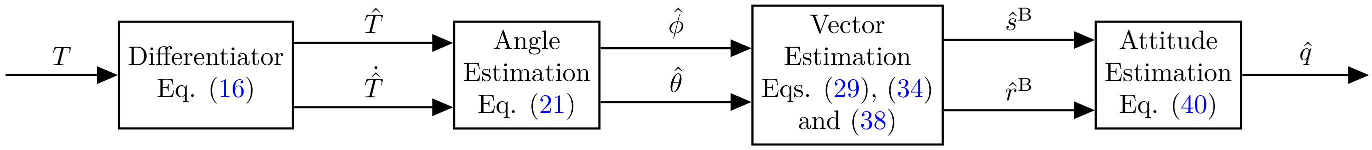

Figure 3: Block diagram of the attitude estimation based on temperature.

5.2. Estimation of the Angle to Sun and Earth

Each pair of temperature sensors with the same normal vector but different coating can be used in order to determine the angle between the normal vector and Sun vector as well as the angle between normal vector and Earth vector. the temperature vectors can be split into T_i with $i \in \{1, \ldots, 6\}$ for black sensors and T_j with $j \in \{7, \ldots, 12\}$ for silver sensors. In the following consider tupel (i, j) are considered with $i \in \{1, \ldots, 6\}$ and $j = i + 6$. The temperature dynamics as introduced in (1) have the form

$$\begin{aligned}\dot{T}_i &= \max\left(\alpha_i \cos(\phi_i), 0\right) + \max(\beta_i F_i, 0) + \gamma_i F_i - \delta_i T_i^4 + \frac{Q_i^{\mathrm{d}}}{C_i} \\ \dot{T}_j &= \max\left(\alpha_j \cos(\phi_j), 0\right) + \max(\beta_j F_j, 0) + \gamma_j F_j - \delta_j T_j^4 + \frac{Q_j^{\mathrm{d}}}{C_j} .\end{aligned} \tag{17}$$

Since i and j were chosen such that they have the same angles, i.e. $\phi_i = \phi_j$ and $F_i = F_j$, the system (17) can be written in matrix form as

$$\begin{bmatrix} \dot{T}_i \\ \dot{T}_j \end{bmatrix} = \begin{bmatrix} \alpha_i & \max(\beta_i, 0) + \gamma_i \\ \alpha_j & \max(\beta_j, 0) + \gamma_j \end{bmatrix} \begin{bmatrix} \max\left(\cos(\phi_i), 0\right) \\ F_i \end{bmatrix} - \begin{bmatrix} \delta_i T_i^4 - \frac{Q_i^{\mathrm{d}}}{C_i} \\ \delta_j T_j^4 - \frac{Q_j^{\mathrm{d}}}{C_j} \end{bmatrix} . \tag{18}$$

For $\alpha_i(\max(\beta_j, 0) + \gamma_j) - \alpha_j(\max(\beta_i, 0) + \gamma_i) \neq 0$ the matrix can be inverted and

$$N_T = \begin{bmatrix} \alpha_i & \max(\beta_i, 0) + \gamma_i \\ \alpha_j & \max(\beta_j, 0) + \gamma_j \end{bmatrix}^{-1} \tag{19}$$

is defined to solve Equation (18) with

$$\begin{bmatrix} \max\left(\cos(\phi_i), 0\right) \\ F_i \end{bmatrix} = N_T \left(\begin{bmatrix} \dot{T}_i \\ \dot{T}_j \end{bmatrix} + \begin{bmatrix} \delta_i T_i^4 - \frac{Q_i^{\mathrm{d}}}{C} \\ \delta_j T_j^4 - \frac{Q_j^{\mathrm{d}}}{C} \end{bmatrix} \right) . \tag{20}$$

The augmented inverse function of the cosine $\overline{\mathrm{acos}} : \mathbb{R} \to [0, \pi]$ is introduced via

$$\overline{\mathrm{acos}}(y) = \begin{cases} \pi & \text{if } y < -1 \\ \mathrm{acos}(y) & \text{if } -1 \leq y \leq 1 \\ 0 & \text{if } y > 1 \end{cases} .$$

Further the inverse of the form factor for a fixed position r is denoted by F^{-1}, i.e. the inverse is defined by $F^{-1} : \mathbb{R} \to [0, \frac{\pi}{2} + \sin^{-1}\left(\frac{r_\oplus}{\|r\|}\right)]$ with $F^{-1}(F(\theta, r)) = \theta$. This inverse can be realised by a simple Newton method due to the monotonicity of F. This inverse can be augmented to obtain

$$\overline{F}^{-1}(y) = \begin{cases} \frac{\pi}{2} + \sin^{-1}\left(\frac{r_\oplus}{\|r\|}\right) & \text{if } y < 0 \\ F^{-1}(y) & \text{if } 0 \leq y \leq \frac{r_\oplus^2}{\|r\|^2} \\ 0 & \text{if } y > \frac{r_\oplus^2}{\|r\|^2} \end{cases} .$$

This allows to define a method to estimate the angles ϕ and θ for a sunlit spacecraft.

Proposition 5.1 *Consider two temperature sensors which dynamics obey Equation (17) with the angles $\phi_i \in [0, \pi]$ and $\theta_i \in [0, \pi]$ as defined in Equation (9). Let $\alpha_i(\max(\beta_j(t), 0) + \gamma_j) - \alpha_j(\max(\beta_i(t), 0) + \gamma_i) \neq 0$. Then the estimate for the angle between the sensor normal and the Sun and Earth is defined to be*

$$\hat{\phi}_i = \overline{\mathrm{acos}} \left(\begin{bmatrix} 1 & 0 \end{bmatrix} N_T \left(\begin{bmatrix} \dot{\hat{T}}_i \\ \dot{\hat{T}}_j \end{bmatrix} + \begin{bmatrix} \delta_i \hat{T}_i^4 - \frac{Q_i^{\mathrm{d}}}{C} \\ \delta_j \hat{T}_j^4 - \frac{Q_j^{\mathrm{d}}}{C} \end{bmatrix} \right) \right) \tag{21a}$$

$$\hat{\theta}_i = \overline{F}^{-1} \left(\begin{bmatrix} 0 & 1 \end{bmatrix} N_T \left(\begin{bmatrix} \dot{\hat{T}}_i \\ \dot{\hat{T}}_j \end{bmatrix} + \begin{bmatrix} \delta_i \hat{T}_i^4 - \frac{Q_i^{\mathrm{d}}}{C} \\ \delta_j \hat{T}_j^4 - \frac{Q_j^{\mathrm{d}}}{C} \end{bmatrix} \right) \right) \tag{21b}$$

for N_T defined in Equation (19). Then, the estimate of the solar angle is exact if the real angle is smaller than $90°$, otherwise the estimate is $90°$, i.e.

$$\hat{\phi}_i = \phi_i \qquad \forall\, \phi_i \leq \frac{\pi}{2} , \tag{22a}$$

$$\hat{\phi}_i = \frac{\pi}{2} \qquad \forall\, \phi_i > \frac{\pi}{2} . \tag{22b}$$

In analog fashion holds for the estimate of the angle between normal and Earth

$$\hat{\theta}_i = \theta_i \qquad \forall\, \theta_i \leq \frac{\pi}{2} + \sin^{-1}\left(\frac{r_\oplus}{\|r\|}\right) , \tag{23a}$$

$$\hat{\theta}_i = \frac{\pi}{2} + \sin^{-1}\left(\frac{r_\oplus}{\|r\|}\right) \qquad \forall\, \theta_i > \frac{\pi}{2} + \sin^{-1}\left(\frac{r_\oplus}{\|r\|}\right) . \tag{23b}$$

Proof: From $0 \leq \phi_i \leq \frac{\pi}{2}$ it follows

$$\begin{aligned}\hat{\phi}_i &= \overline{\mathrm{acos}} \left(\begin{bmatrix} 1 & 0 \end{bmatrix} N_T \left(\begin{bmatrix} \dot{\hat{T}}_i \\ \dot{\hat{T}}_j \end{bmatrix} + \begin{bmatrix} \delta_i \hat{T}_i^4 - \frac{Q_i^{\mathrm{d}}}{C} \\ \delta_j \hat{T}_j^4 - \frac{Q_j^{\mathrm{d}}}{C} \end{bmatrix} \right) \right) \\ &\overset{(20)}{=} \overline{\mathrm{acos}}(\max(\cos(\phi_i), 0)) \overset{\phi_i \in [0, \frac{\pi}{2}]}{=} \overline{\mathrm{acos}}(\cos(\phi_i)) = \phi_i\end{aligned}$$

and the claim (22a) is shown. For $\frac{\pi}{2} < \phi_i < \pi$ it is

$$\hat{\phi}_i = \overline{\text{acos}}\left(\begin{bmatrix}1 & 0\end{bmatrix} N^\top \left(\begin{bmatrix}\dot{\hat{T}}_i \\ \dot{\hat{T}}_j\end{bmatrix} + \begin{bmatrix}\delta_i \hat{T}_i^4 - \frac{Q_i^{\mathrm{d}}}{C} \\ \delta_j \hat{T}_j^4 - \frac{Q_j^{\mathrm{d}}}{C}\end{bmatrix}\right)\right) \tag{24}$$

$$\overset{(20)}{=} \overline{\text{acos}}(\max(\cos(\phi_i), 0)) \overset{\phi_i(q)\in(\frac{\pi}{2},\pi]}{=} \overline{\text{acos}}(0) = \frac{\pi}{2} \tag{25}$$

and the claim (22b) is shown. The claims (23a) and (23b) can be shown in analogue fashion. □

The proposition has shown that it must be distinguished between the two cases whether the side is pointing into the direction of the heat source or not. Equation (22a) ensures that for a sensor pointing into the direction of the Sun, i.e. $\phi \leq \frac{\pi}{2}$, the estimate is accurate. However, for a sensor pointing away from the Sun as in Equation (22b), i.e. $\phi \in (\frac{\pi}{2}, \pi]$ the estimated angle is always $\frac{\pi}{2}$. In this case, this estimate is generally not useful to estimate the attitude. Similar results are obtained for the angle to Earth but the critical angle is higher, due to the Earth being considered as a spherical heat source and not a point heat source. These step is also the step where potential model uncertainties are propagated. Uncertainties in Q^{d} and the parameters leads to error in the angle estimation. However, these errors are small if the model uncertainties are small which can be ensured by an appropriate system identification.

5.3. Estimation of the Sun and Earth Vector in Body Frame

Two tasks need to be solved. First, the angles that contain actual information to determine the desired vectors must be found. Second, the vectors of Sun and Earth must be calculated from these angles. The beginning is made by solving the second task as this shows the information that is required to calculate the angles.

5.3.1. Calculation of Sun and Earth Vector in Body Frame from Solar Angles

From the definition of ϕ_i and θ_i according to Equation (9) the system of equations is defined as

$$\frac{s^\top}{\|s\|} A(q)^\top n_i = \cos(\phi_i) \quad i \in \{1, \dots 6\} \tag{26a}$$

$$-\frac{r^\top}{\|r\|} A(q)^\top n_i = \cos(\theta_i) \quad i \in \{1, \dots 6\}\,. \tag{26b}$$

The matrix of normal vectors is denoted by $N = [n_1, \dots, n_6] \in \mathbb{R}^{3\times 6}$, the vector of cosines of the angle between Sun and normal by $b_\phi = [\cos(\phi_1), \dots \cos(\phi_6)]^\top \in \mathbb{R}^6$ and the vector of the cosines of the angles between normal and Earth by $b_\theta = [\cos(\theta_1), \dots \cos(\theta_6)]^\top \in \mathbb{R}^6$. With $b_{\hat{\phi}}$ and $b_{\hat{\theta}}$ the vectors b_ϕ and b_θ with $\phi = \hat{\phi}$ and $\theta = \hat{\theta}$ are denoted, respectively. Then Equation (26a) can be written as

$$\frac{s^\top}{\|s\|} A(q)^\top N = b_\phi^\top\,.$$

Transposing both sides leads to

$$N^\top A(q) \frac{s}{\|s\|} = b_\phi\,. \tag{27}$$

It is aimed to replace b_ϕ by the estimate $b_{\hat{\phi}}$ and formulate a conventional attitude estimation problem in the sense of Wahba Markley and Crassidis (2014). Therefore, the system of equations needs to be solved for $A(q)s \in \mathbb{R}^3$. Clearly, this is an overdetermined linear system of equations with six equations and three variables. For an imperfect model and measurements the system has no solution but needs to be considered as an optimisation problem. However, generally not all of the estimates are sensible for the reconstruction as discussed in the previous section. Thus, a positive semi-definite diagonal weight matrix $W_\phi = [w_{\phi,1}, \dots w_{\phi,6}]^\top \in \mathbb{R}^{6\times 6}$ is multiplied to the system that decides which of the measurements should be taken into account. The weight matrix is chosen such that $W_\phi N^\top$ has full rank 3. The choice of its individual entries will be discussed in the next Section 5.3.2. It is continued by showing how to estimate the vectors in body frame and show that the estimate is correct for a perfect model and measurements.

Proposition 5.2 *Consider two temperature sensors which dynamics obey Equation (17) and the assumptions and angle estimations as in (21). Further let W_ϕ and W_θ be positive semi-definite diagonal matrices such that $W_\phi N^\top$ and $W_\theta N^\top$ have full rank and fulfil*

$$w_{\phi,i} = 0 \qquad \forall\, \phi_i > \frac{\pi}{2} \tag{28a}$$

$$w_{\theta,i} = 0 \qquad \forall\, \theta_i > \frac{\pi}{2} + \sin^{-1}\left(\frac{r_\oplus}{\|r\|}\right) \tag{28b}$$

for $i \in \{1, \dots 6\}$.

Then the estimated vectors

$$\hat{s}^{\mathrm{B}} := (W_\phi N^\top)^+ W_\phi b_{\hat{\phi}} \|s\| \tag{29a}$$

$$\hat{r}^{\mathrm{B}} := -(W_\theta N^\top)^+ W_\theta b_{\hat{\theta}} \|r\| \tag{29b}$$

are the Earth and the Sun vector in body coordinates, i.e.

$$\hat{s}^{\mathrm{B}} = A(q)s \qquad\qquad \hat{r}^{\mathrm{B}} = A(q)r\,. \tag{30}$$

Proof: The solution of (27) exists by definition of ϕ. Because N has full rank, the solution of (27) is unique. Multiplying the weight matrix W_ϕ to both sides in (27) yields

$$W_\phi N^\top A(q) \frac{s}{\|s\|} = W_\phi b_\phi\,. \tag{31}$$

Condition (28a) ensures with Equation (22a) and the diagonal form of W_ϕ that

$$e_i^\top W_\phi b_\phi = w_{\phi,i}^\top b_\phi = w_{\phi,i}^\top b_{\hat{\phi}} = e_i^\top W_\phi b_{\hat{\phi}}$$

for all $i \in \{1, \dots 6\}$. The equality in the middle holds because $w_{\phi,i}$ is either a multiple of the i-th unit vector

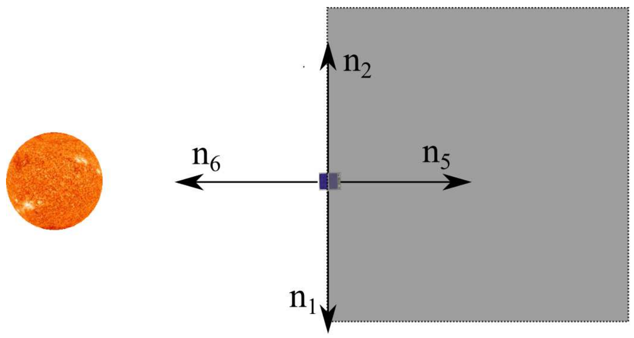

Figure 4: Illustration of the planar projection of the Sun, spacecraft and its normals.

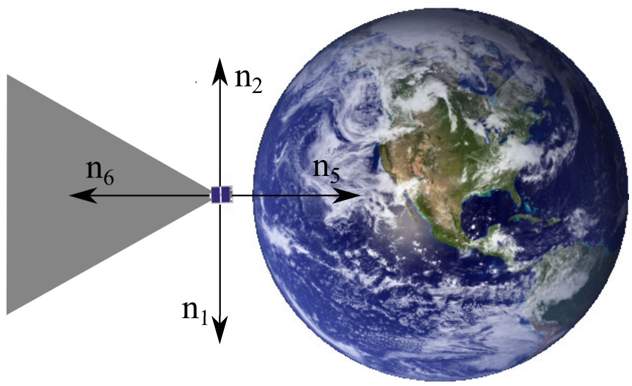

Figure 5: Illustration of the planar projection of the Earth, spacecraft and its normals.

resulting in $\cos(\phi_i) = \cos(\hat{\phi}_i)$ or identical to zero. Consequently, the equation $W_\phi b_\phi = W_\phi b_{\hat{\phi}}$ holds. Multiplying $NW_\phi^\top$ from the left side to obtain a quadratic matrix yields

$$NW_\phi^\top W_\phi N^\top A(q)\frac{s}{\|s\|} = NW_\phi^\top W_\phi b_{\hat{\phi}}\,.$$

The inverse of $NW_\phi^\top W_\phi N^\top$ exists because $W_\phi N^\top$ has full rank. Multiplying with the inverse and $\|s\|$ from the left side leads to Equation (29) and (30). The same arguments can be made for θ and $A(q)\frac{-r}{\|r\|}$. □

This proposition in Equation (28) has provided the requirements that need to be met by the weight matrix and has shown in (30) that the resulting estimation of the vectors in body frame is accurate. Note that for an imperfect model and measurements, the estimation is still optimal as stated in the following formulation.

Remark 1 *The estimates of the solar and the Earth vector in body frame $\hat{s}^{\mathrm{B}}$, $\hat{r}^{\mathrm{B}}$ obtained from (29) are the best possible solutions in that sense, that they are the least square solutions which solve the optimisation problem*

$$\min_{\hat{s}^{\mathrm{B}},\hat{r}^{\mathrm{B}}} \quad e_1^\top e_1 + e_2^\top e_2 \tag{32a}$$

$$s.\ t. \quad e_1 = W_\phi N^\top \frac{\hat{s}^{\mathrm{B}}}{\|s\|} - W b_{\hat{\phi}} \tag{32b}$$

$$e_2 = W_\theta N^\top \frac{\hat{r}^{\mathrm{B}}}{\|r\|} - W b_{\hat{\theta}} \tag{32c}$$

resulting from (31).

Proposition (5.2) assumes that enough of the twelve measurements provide useful information to estimate the Earth and Sun vectors in body frame i.e. the existence of the weight matrices W_ϕ, W_θ to fulfil the rank condition. It can be shown that there exists such a weight matrix and that the choice of the weight matrix influences the quality of the solution. This is interrogated in the following and completes this section.

5.3.2. Choice of the Weight Matrices

As established in the previous section, the choice of the weight matrix means to choose the estimated angles that are of use for the attitude estimation. The choice of this matrix varies with the configuration of the sensor up to the point that the matrices do not necessarily exist if the configuration is chosen poorly. In the case of a cuboid configuration, the sensors are pointing along each of the unit vectors which ensures the existence of the weight matrices. There is basically no design freedom for the choice of the weight matrix W_ϕ as illustrated in Figure 4 which shows the planar projection of the Sun, spacecraft and its normals. The Sun is depicted to be very small, instead of displaying the large distance between Sun and spacecraft. Thus, the Sun can be considered a point heat source and the spacecraft surfaces as infinitesimal small. This leads to the black half-plane which describes the normals of the surfaces for which there is no exposure to solar irradiation. In the depicted case three normal vectors are inside the plane and one is outside. In all other cases every rotation leads to exactly two normal vectors inside the plane and two outside. With the additional vector for the third dimension not displayed in the illustration this leads to exactly three normal vectors outside the half-plane which is the minimum of information required to estimate the Sun position. More design freedom exists for the choice of W_θ as illustrated in Figure 5 by the planar projection of the Earth, spacecraft and its normals. The Earth is considered as a spherical heat source and the spacecraft surfaces as infinitesimal small. For the considered orbits, the critical angle θ_{crit} is around 150 deg resulting in the black cone with an angle of about 60 degrees which describes the normals for which no infrared and albedo irradiation acts on the surface. It can be seen that for all spacecraft orientations at most one normal vector lies inside the cone. Therefore most pairs of positive and negative unit vectors contain redundant information that can be used in an optimal manner to estimate the position of the Earth. A mathematically more profound and detailed description of these properties and design for both weight matrices is proposed in the following.

It is started with the weight matrix W_ϕ for the Sun vector estimation. Naturally, any measurement that gives information about the location of the Sun as also used in

Equation (22a) and (28) should be weighed. Therefore, the choice of the six normal vectors leads to a matrix of rank three which is defined in the following way

$$w_{\phi,i}(\phi) = \begin{cases} e_i & \text{if } \phi_i \leq \frac{\pi}{2} \\ 0 & \text{otherwise} \end{cases} \tag{33}$$

where e_i is the i-th six dimensional unit vector. This matrix is uniquely defined and there is no real way to optimise it. Changing the weights that are identical to zero would lead to the usage of undesired information while changing the non-zero weights does not change the solution as they weigh independent variables. Only in the special case $\phi_i = \phi_{i+1} = \frac{\pi}{2}$ changing the weights to $w_{\phi,i}(\phi) = a_i e_i$ and $w_{\phi,i+1}(\phi) = (1 - a_i)e_{i+1}$ with the parameter $a_i \in [0, 1]$ would be sensible. The more accurate measurement should obtain a higher weight.

As the exact angle ϕ is not known but only its estimate $\hat{\phi}$ which is generally subject to model uncertainties and measurement errors, it is not advisable to use equation (33) with $\phi = \hat{\phi}$ to define the weight matrix. Instead, it must be ensured that only one of the two in the opposite direction pointing sides is used as formulated in the following proposition.

Proposition 5.3 *Consider the assumptions and angle estimates as in* (21). *Then, the choice of the weights as*

$$w_{\phi,i}(\hat{\phi}_i) = \begin{cases} e_i & \text{if } \min(\hat{\phi}_i, \hat{\phi}_{i+1}) = \hat{\phi}_i \\ & \quad \text{or } \hat{\phi}_i = \hat{\phi}_{i+1} \text{ for } i \in \{1, 3, 5\} \\ e_i & \text{if } \min(\hat{\phi}_{i-1}, \hat{\phi}_i) = \hat{\phi}_i \\ & \quad \text{or } \hat{\phi}_{i-1} = \hat{\phi}_i \text{ for } i \in \{2, 4, 6\} \\ 0 & \text{otherwise} \end{cases} \tag{34}$$

ensures that the matrix $W_\phi N^\top$ has full rank and it is

$$\phi_i > \frac{\pi}{2} \Rightarrow w_{\phi,i} = 0\,. \tag{35}$$

Proof: Due to the structure of N and the definition of ϕ establish the connection between ϕ_{i+1} and ϕ_i can be established as

$$\phi_{i+1} = \pi - \phi_i \tag{36}$$

for $i = \{1, 3, 5\}$. This shows that at least one of the two sensors i and $i+1$ is under the influence of sunlight. Consequently, for the estimation holds according to Proposition 5.1 that either ϕ_i or ϕ_{i+1} are estimated correctly and smaller than $\frac{\pi}{2}$ or both are estimated correctly and identical to $\frac{\pi}{2}$. Thus, the definition of W_ϕ in (34) ensures that the matrix $W_\phi N$ has full rank as its rows consist of all three unit vectors, because

$$W_\phi N^\top e_i = e_i \qquad W_\phi N^\top e_{i+1} = -e_i$$

for $i \in \{1, 3, 5\}$.

It remains to prove the claim (35). Suppose there is $i \in \{1, 3, 5\}$ with $\phi_i > \frac{\pi}{2}$. Then $\hat{\phi}_i = \frac{\pi}{2}$ and $\hat{\phi}_{i+1} < \frac{\pi}{2}$ and consequently the definition of the weight matrix (34) yields $w_{\phi,i} = 0$. The same argument can be made for $\phi_i > \frac{\pi}{2}$ with $i \in \{2, 4, 6\}$. □

This proposition has given a suitable choice of W_ϕ to ensure the requirements of the weight matrix W_ϕ imposed in Proposition 5.2.

For W_θ the choice of the weights is less straightforward because the influence of θ is propagated by the form factor F and not the cosine. The critical angle $\theta_{\text{crit}} = \frac{\pi}{2} + \sin^{-1}\left(\frac{r_\oplus}{\|r\|}\right)$ is approximately $\frac{5}{6}\pi \approx 150°$ for the considered orbit. Consequently, at least five out of the six sensors provide information that can be used to estimate $A(q)r$ at all times. For a perfect model and measurements it is simple to determine whether a measurement should be incorporated. If $\hat{\theta}_i \geq \theta_{\text{crit}}$ and $\pi - \hat{\theta}_{i+1} \leq \theta_{\text{crit}}$ the angle should not be incorporated into the design for $i \in \{1, 3, 5\}$. A simple robust approach always uses five of the six measurements for the attitude estimation.

Proposition 5.4 *Consider the assumptions and angle estimates as in* (21). *Suppose that $\theta_{\text{crit}} > \frac{3}{4}\pi$ and find the index k of the highest angle which fulfils*

$$\hat{\theta}_k = \max_{i=1\ldots6} \hat{\theta}_i\,. \tag{37}$$

Choose the weight matrix as

$$w^{\text{no}}_{\theta,i}(\hat{\theta}_i) = \begin{cases} \alpha_{\frac{i+1}{2}} e_i & \text{if } i \in \{1, 3, 5\} \setminus \{k\} \\ (1 - \alpha_{\frac{i}{2}})e_i & \text{if } i \in \{2, 4, 6\} \setminus \{k\} \\ 0 & \text{if } i = k\,. \end{cases} \tag{38}$$

for some design parameters $\alpha_1, \alpha_2, \alpha_3 \in [0, 1]$. Then the matrix $W_\theta N^\top$ has full rank and

$$\theta_i > \frac{\pi}{2} + \sin^{-1}\left(\frac{r_\oplus}{\|r\|}\right) \Rightarrow w_{\theta,i} = 0$$

holds.

Proof: The full rank of the matrix $W_\theta N^\top$ is clear. Since $\theta_{\text{crit}} > \frac{3}{4}\pi$ there is at most one θ_i such that $\theta_i > \theta_{\text{crit}}$ because $\min_{i,j \in \{1,\ldots6\}, j \neq i} \angle(n_i, n_j) = \frac{\pi}{2}$. If there is k such that $\theta_k > \theta_{\text{crit}}$, then it is $\hat{\theta}_k = \theta_{\text{crit}}$ and consequently $\hat{\theta}_k = \max_{i=1\ldots6} \hat{\theta}_i$. Because all the other estimates are exact $\hat{\theta}^{\text{no}}_k = \theta_k > \theta_{\text{crit}}$ is obtained and therefore $w_{\theta,k}(\hat{\theta}_k) = 0$. □

This Proposition has given a choice of the weight matrix W_θ that ensures the requirements for Proposition (5.2). As shown in the proposition, the k-th measurement is never required to estimate the attitude, as the remaining five measurements are sufficient to generate a valid estimate of q. However, this measurement can improve the estimation if $\theta_k < \theta_{\text{crit}}$. The incorporation of this measurement is discussed in Posielek (2022). The next section shows how to obtain the attitude estimation from the two body vectors.

5.4. Attitude Estimation from the Vectors in Body Frame

Obtaining the attitude from two vectors in body frame is a standard problem and sufficiently analysed in the literature Markley and Crassidis (2014); Canuto et al. (2018). In this section it is merely show how the problem is transformed into the standard problem and stated how this is commonly solved.

From Equation (27) follows that the equation

$$A(q)\frac{s}{\|s\|} = \frac{s^{\mathrm{B}}}{\|s^{\mathrm{B}}\|} \qquad A(q)\frac{r}{\|r\|} = \frac{r^{\mathrm{B}}}{\|r^{\mathrm{B}}\|} \tag{39a}$$

holds with

$$s^{\mathrm{B}} = (N^\top)^{+} b_\phi \|s\| \qquad r^{\mathrm{B}} = -(N^\top)^{+} b_\theta \|r\|$$

where $\|s^{\mathrm{B}}\| = \|s\|$ and $\|r^{\mathrm{B}}\| = \|r\|$. Estimating the attitude matrix of these systems of equations can be cast into the formulation of Wahba's problem which is commonly referred to in literature, e.g. Markley and Crassidis (2014). Any of the algorithms that maps the estimated vectors in initial and body coordinates to the desired attitude q is denoted by f^{Wahba}. For the analysis and the observer proof it is not important if a simple TRIAD algorithm or more complicated methods such as Davenport's q-Method or QUEST are chosen.

Proposition 5.5 *Consider the assumptions and estimates from Proposition (5.2). Then the estimate*

$$\hat{q} = f^{\mathrm{Wahba}}\left(\begin{bmatrix}\frac{s}{\|s\|} & \frac{r}{\|r\|}\end{bmatrix}^\top, \begin{bmatrix}\frac{\hat{s}^{\mathrm{B}}}{\|\hat{s}^{\mathrm{B}}\|} & \frac{\hat{r}^{\mathrm{B}}}{\|\hat{r}^{\mathrm{B}}\|}\end{bmatrix}^\top\right) \tag{40}$$

represents the current attitude, i.e.

$$A(q) = A(\hat{q})\,. \tag{41}$$

Proof: Due to Proposition (5.2) it is $\hat{r}^{\mathrm{B}} = r^{\mathrm{B}}$ and $\hat{s}^{\mathrm{B}} = s^{\mathrm{B}}$. Consequently, $\hat{q}$ is a solution of Equation (39) which leads directly to the claim. □

5.5. Complete Observer

The complete algorithm has the form as displayed in Figure 3. The right hand side of (21) is denoted as $f_i^{\mathrm{Ang}}(T_i, \dot{T}_i)$, the right hand side of (29) with the gain matrix defined in (34) and (38) by $f^{\mathrm{Vec}}(\hat{\phi}_1, \hat{\theta}_1, \ldots, \hat{\phi}_{12}, \hat{\theta}_{12})$ and the right hand side of (40) by $f^{\mathrm{Quat}}(\hat{s}_B, \hat{r}_B)$. Then the algorithm can be cast into the form of (15) as

$$\frac{\mathrm{d}}{\mathrm{d}t}\begin{bmatrix}\hat{T}_1\\ \dot{\hat{T}}_1\\ \vdots\\ \hat{T}_{12}\\ \dot{\hat{T}}_{12}\end{bmatrix} = \mathrm{diag}\left(\begin{bmatrix}0 & 1\\ 0 & 0\end{bmatrix}, \ldots, \begin{bmatrix}0 & 1\\ 0 & 0\end{bmatrix}\right)\begin{bmatrix}\hat{T}_1\\ \dot{\hat{T}}_1\\ \vdots\\ \hat{T}_{12}\\ \dot{\hat{T}}_{12}\end{bmatrix} + \mathrm{diag}\left(\begin{bmatrix}\frac{a_1}{\varepsilon}\\ \frac{a_0}{\varepsilon^2}\end{bmatrix}, \ldots, \begin{bmatrix}\frac{a_1}{\varepsilon}\\ \frac{a_0}{\varepsilon^2}\end{bmatrix}\right)\begin{bmatrix}T_1 - \hat{T}_1\\ \vdots\\ T_{12} - \hat{T}_{12}\end{bmatrix} \tag{42a}$$

$$\hat{q} = f^{\mathrm{Quat}}\Big(f^{\mathrm{Vec}}\big(f_1^{\mathrm{Ang}}(\hat{T}_1, \dot{\hat{T}}_1), \ldots, f_{12}^{\mathrm{Ang}}(\hat{T}_{12}, \dot{\hat{T}}_{12})\big)\Big)\,. \tag{42b}$$

It can be seen that the dynamic part of the observer (42a) is simple and linear, as it estimates only the derivatives of the temperature measurements. All the non-linearities of the observer are found in the transformation (42b) from the temperature derivatives to the attitude. Note, that the proposed observer uses only the measurements of the temperatures T and neither the angular velocity measurement ω nor the input u. Additionally, the temperature dynamics (14a)-(14c) are used to estimate the attitude $\hat{q}$ but neither the quaternion nor the angular velocity dynamics (14d) or (14e) are required for the estimation. This leaves space for improvements and augmentations of the algorithm as discussed in the upcoming section.

6. Adaptation of the Algorithm

In this section an additional filter is proposed which uses the angular velocity measurements to refine the attitude estimation. Further, the case when the spacecraft is in solar eclipse and the previously introduced observer cannot be applied because the matrix N_T is not invertible any more is considered.

6.1. Additional Attitude Filter

In order to smooth the attitude estimation, an additional attitude filter can be used to obtain a filtered estimation $\hat{q}^{\mathrm{fil}}$ from the estimation $\hat{q}$. The form of this filter may vary. A non-linear quaternion filter in the spirit of Tayebi (2008) is proposed as

$$\dot{\hat{q}}_{\mathrm{fil}} = \frac{1}{2}\Xi(\hat{q}_{\mathrm{fil}})\hat{\omega} + k\frac{1}{2}\Xi(\hat{q})\Xi^\top(\hat{q}_{\mathrm{fil}})\hat{q} \tag{43}$$

because it allows a simple adaptation of the gain $k \in \mathbb{R}$. This requires a good measurement or estimation of the angular velocity $\hat{\omega}$.

6.2. Spacecraft in Solar Eclipse

For the spacecraft in solar eclipse no solar or albedo irradiation is acting. Thus, Equation (18) simplifies to

$$\begin{bmatrix}\gamma_i\\ \gamma_j\end{bmatrix} F(\theta_i(q,r,n_i),r) = \left(\begin{bmatrix}\dot{\hat{T}}_i\\ \dot{\hat{T}}_j\end{bmatrix} + \begin{bmatrix}\delta_i\hat{T}_i^4 - \frac{Q_i^{\mathrm{d}}}{C_i}\\ \delta_j\hat{T}_j^4 - \frac{Q_j^{\mathrm{d}}}{C_j}\end{bmatrix}\right) . \quad (44)$$

Thus, the angle between normal and Sun cannot be estimated. However, the angle between normal and Earth can be estimated more accurately.

Proposition 6.1 *Consider two temperature sensors which dynamics obey Equation (17) with the angles $\phi \in [0,\pi]$ and $\theta \in [0,\pi]$ as defined in Equation (26). Let the spacecraft be in solar eclipse, i.e. $\alpha_i, \beta_i = 0$ but with acting infrared irradiation, i.e. with either $\gamma_i \neq 0$ or $\gamma_{i+6} \neq 0$ or both. Then an estimate for the angle between the normal and the Earth is obtained using*

$$\hat{\theta}_i = \overline{F}^{-1}\left(\begin{bmatrix}\gamma_i\\ \gamma_j\end{bmatrix}^+ \left(\begin{bmatrix}\dot{\hat{T}}_i\\ \dot{\hat{T}}_j\end{bmatrix} + \begin{bmatrix}\delta_i\hat{T}_i^4 - \frac{Q_i^{\mathrm{d}}}{C}\\ \delta_j\hat{T}_j^4 - \frac{Q_j^{\mathrm{d}}}{C}\end{bmatrix}\right)\right) . \quad (45a)$$

For the estimate of the angle between normal and Earth holds

$$\theta_i \leq \frac{\pi}{2} + \sin^{-1}\left(\frac{r_\oplus}{\|r\|}\right) \Rightarrow \hat{\theta}_i = \theta_i \quad (46a)$$

$$\theta_i > \frac{\pi}{2} + \sin^{-1}\left(\frac{r_\oplus}{\|r\|}\right) \Rightarrow \hat{\theta}_i = \frac{\pi}{2} + \sin^{-1}\left(\frac{r_\oplus}{\|r\|}\right) . \quad (46b)$$

Proof: Analogue to Proposition 5.1 using the solution of Equation (44). □

In this case, the functions developed in 5.3 and 5.4 cannot be employed due to the missing angle. The simplest solution to this issue is to use the attitude filter (43) with $k = 0$ to propagate the estimated attitude for the period of the eclipse. Different observer structures can also rely on the separation of the attitude into the part that is defined by these Earth angles θ and a rest. The θ-part can then be corrected using the estimation (45) while the rest can be propagated using the underlying dynamics and angular velocity measurements. This method is not discussed in this work but can be obtained using an observer in natural coordinates as discussed in Posielek (2022).

7. Attitude Estimation under Sensor Outage

In this section sensor outages are considered. Due to the pairs of black and silver sensors often physically attached to each other a failure of both of them is assumed. Further, it is assumed that the malfunctioning sensors are detected and removed from the sensor configuration immediately.

7.1. Problem Definition

Consider a new configuration $\bar{N}^{\mathrm{con}} \subsetneq N^{\mathrm{con}}$ such that only a subset of the Equations (14a) - (14c) holds. As discussed in Section 5, the original configuration N^{con} is chosen such that a reconstruction of the attitude is possible at all times for a spacecraft not in eclipse. This is due to the fact that for all possible attitudes at least three sensors are simultaneously sunlit as shown in Proposition 5.3. This cannot be guaranteed for the resulting failure configuration which means that the algorithm introduced in Section 5.3 cannot be applied. Thus the original algorithm is adapted to determine all possible attitudes. The methods presented in Section 5.1 and 5.2 allow to estimate the angles $\hat{\phi}, \hat{\theta}$. These can be used to define the set of normals with the correctly estimated angles

$$\hat{\mathcal{N}}_\phi^{\mathrm{ld}}(q) = \{n_i \in \bar{N}^{\mathrm{con}} \mid i \in \{1,\dots,12\} : \hat{\phi}_i < \frac{\pi}{2}\} \quad (47a)$$

$$\hat{\mathcal{N}}_\theta^{\mathrm{ld}}(q) = \{n_i \in \bar{N}^{\mathrm{con}} \mid i \in \{1,\dots,12\} : \hat{\theta}_i < \theta^{\mathrm{crit}}\} \quad (47b)$$

at the attitude q where the superscript $\cdot^{\mathrm{ld}}$ shall emphasis that these sets can be linear dependent. Out of these sets linear independent subsets $\hat{\mathcal{N}}_\phi(q) \subset \hat{\mathcal{N}}_\phi^{\mathrm{ld}}(q)$ and $\hat{\mathcal{N}}_\theta(q) \subset \hat{\mathcal{N}}_\theta^{\mathrm{ld}}(q)$ can be constructed. These allow to directly correlate the designed algorithm to a number of possible attitudes with the cardinality of the sets $\hat{\mathcal{N}}_\phi(q)$ and $\hat{\mathcal{N}}_\theta(q)$. According to their definition, the linear dependence of the sets $\hat{\mathcal{N}}_\phi^{\mathrm{ld}}(q), \hat{\mathcal{N}}_\theta^{\mathrm{ld}}(q)$ may occur if they contain a pair (n_i, n_{i+1}) for $i \in \{1,3,5\}$. A linear independent subset $\hat{\mathcal{N}}_\phi(q)$ is constructed by simply replacing the pair using the smaller of the two angles. This is done in analogue fashion to obtain $\hat{\mathcal{N}}_\theta$ and for the sets containing the real normals $\mathcal{N}_\phi$ and $\mathcal{N}_\theta$.

In order to use the individual elements, they are denoted as $\hat{\mathcal{N}}_\phi(q) = \{n_{i_1},\dots,n_{i_{m^\phi}}\}$ and $\hat{\mathcal{N}}_\theta(q) = \{n_{j_1},\dots,n_{j_{m^\theta}}\}$ where $m^\phi, m^\theta \in \{0,1,2,3\}$ denote the cardinality of $\hat{\mathcal{N}}_\phi(q)$ and $\hat{\mathcal{N}}_\theta(q)$, respectively, and $i_k, j_l \in \{1,\dots,6\}$ the index of the normal vectors for $k \in \{1,\dots,m^\phi\}$ and $l \in \{1,\dots,m^\theta\}$ with $i_k < i_{k+1}$ and $j_l < j_{l+1}$. In other words, the remaining functional sensors are split into the linear independent sensors $n_{i_1},\dots,n_{i_{m^\phi}}$ that can be used to estimate the angle to sun ϕ_{i_k} and the linear independent sensors $n_{j_1},\dots,n_{j_{m^\theta}}$ that allow an estimation of the angle to earth θ_{i_k}. The number of linear independent sensors from which the angle to sun ϕ_{i_k} can be reconstructed is denoted by m^ϕ while the number of linear independent sensors from which the angle to earth θ_{j_l} can be reconstructed is denoted by m^θ.

Following the algorithm from the previous Section 5 requires to estimate the Sun and Earth vector in body frame $s^{\mathrm{B}}, r^{\mathrm{B}}$ and the final estimation of the attitude as discussed in Section 5.4. While the latter method does not change, the first task must now be fulfilled with fewer correctly estimated angles. In order to achieve this, it is helpful to use $s^{\mathrm{B}} = A(\hat{q})s$, $\hat{r}^{\mathrm{B}} = A(\hat{q})r$ to obtain the norm constraints

$$\|\hat{s}^{\mathrm{B}}\| = \|s\| , \qquad \|\hat{r}^{\mathrm{B}}\| = \|r\| , \quad (48)$$

the angle constraint

$$\hat{s}^{\mathrm{B}\top}\hat{r}^{\mathrm{B}} = s^\top r\,, \tag{49}$$

and with Equation (22b) and (23b) the constraints for angles that were not used in the estimation process

$$n_j^\top \hat{s}^{\mathrm{B}} < 0 \qquad \forall\, n_j \in \bar{N}^{\mathrm{con}} \setminus \hat{\mathcal{N}}_\phi^{\mathrm{ld}}(q)\,, \tag{50a}$$
$$n_j^\top \frac{\hat{r}^{\mathrm{B}}}{\|r\|} < \cos(\theta^{\mathrm{crit}}) \qquad \forall\, n_j \in \bar{N}^{\mathrm{con}} \setminus \hat{\mathcal{N}}_\theta^{\mathrm{ld}}(q)\,. \tag{50b}$$

Note that these Equations are written in the estimated variables $\hat{s}^{\mathrm{B}}$, $\hat{r}^{\mathrm{B}}$ but they also hold for the real variables s^{B}, r^{B}.

Consequently, the problem of sensor outage can be considered as solving the system of Equations

$$\begin{matrix} \hat{s}^{\mathrm{B}\top} n_{i_1} = \cos(\hat{\phi}_{i_1})\|s\| & \hat{r}^{\mathrm{B}\top} n_{j_1} = \cos(\hat{\theta}_{j_1})\|r\| \\ \vdots & \vdots \\ \hat{s}^{\mathrm{B}\top} n_{i_{m^\phi}} = \cos(\hat{\phi}_{i_{m^\theta}})\|s\| & \hat{r}^{\mathrm{B}\top} n_{j_{m^\theta}} = \cos(\hat{\theta}_{j_{m^\theta}})\|r\| \end{matrix} \tag{51}$$

combined with (48) and (49) for the vectors $\hat{s}^{\mathrm{B}}, \hat{r}^{\mathrm{B}}$ under the constraints (50).

7.2. Observer Design

Without loss of generality, it is assumed that $|\hat{\mathcal{N}}_\theta| \geq |\hat{\mathcal{N}}_\phi|$. If this condition does not hold, the proposed methods can be executed switching the variables $\hat{r}^{\mathrm{B}}$ and $\hat{s}^{\mathrm{B}}$. The system of equations (48), (49) and (51) has six variables and up to nine equations. However, due to the nonlinearity of the Equations (48) and (49) it is not straightforward to determine the solvability of the system nor the solutions itself. The existence and way to determine the solutions depends on the cardinality of $\hat{\mathcal{N}}_\phi$ and $\hat{\mathcal{N}}_\theta$.

7.2.1. $|\hat{\mathcal{N}}_\theta| = 3$ and $|\hat{\mathcal{N}}_\phi| = 3$

In this case the system of equations (51) is linear and can be represented by a quadratic matrix of full rank. Thus simple inversion leads to the desired vectors.

7.2.2. $|\hat{\mathcal{N}}_\theta| = 3$ and $|\hat{\mathcal{N}}_\phi| = 2$

The Earth vector in body frame $\hat{r}^{\mathrm{B}}$ is easily accessed solving the linear system (51). The remaining two equations of (51) are

$$n_{i_1}^\top \hat{s}^{\mathrm{B}} = \cos(\hat{\phi}_{i_1})\|s\| \qquad n_{i_2}^\top \hat{s}^{\mathrm{B}} = \cos(\hat{\phi}_{i_2})\|s\|\,. \tag{52}$$

Then, $i_3 \in \{1,\dots,6\}$ can be chosen such that $N = [n_{i_1}\ n_{i_2}\ n_{i_3}]$ is an orthonormal matrix. Then Equation (49) is used which has the form

$$r^\top s = \hat{r}^{\mathrm{B}\top}\hat{s}^{\mathrm{B}} = \hat{r}^{\mathrm{B}\top} N N^\top \hat{s}^{\mathrm{B}} \tag{53}$$
$$= \hat{r}^{\mathrm{B}\top} n_{i_1} n_{i_1}^\top \hat{s}^{\mathrm{B}} + \hat{r}^{\mathrm{B}\top} n_{i_2} n_{i_2}^\top \hat{s}^{\mathrm{B}} + \hat{r}^{\mathrm{B}\top} n_{i_3} n_{i_3}^\top \hat{s}^{\mathrm{B}}\,. \tag{54}$$

This can be reformulated to obtain the third component

$$n_{i_3}^\top \hat{s}^{\mathrm{B}} = \frac{r^\top s - \hat{r}^{\mathrm{B}\top} N e_1 n_{i_1}^\top \hat{s}^{\mathrm{B}} - \hat{r}^{\mathrm{B}\top} N e_2 n_{i_2}^\top \hat{s}^{\mathrm{B}}}{\hat{r}^{\mathrm{B}\top} n_{i_3}} \tag{55a}$$
$$= -\frac{\hat{r}^{\mathrm{B}\top} n_{i_2}}{\hat{r}^{\mathrm{B}\top} n_{i_3}} n_{i_2}^\top \hat{s}^{\mathrm{B}} + \frac{r^\top s - \hat{r}^{\mathrm{B}\top} n_{i_1} n_{i_1}^\top \hat{s}^{\mathrm{B}}}{\hat{r}^{\mathrm{B}\top} n_{i_3}}\,. \tag{55b}$$

Then the Sun vector in body frame is obtained using (52) and (55) with

$$\hat{s}^{\mathrm{B}} = N N^\top \hat{s}^{\mathrm{B}} = N[n_{i_1}^\top \hat{s}^{\mathrm{B}},\, n_{i_2}^\top \hat{s}^{\mathrm{B}},\, n_{i_3}^\top \hat{s}^{\mathrm{B}}]^\top\,. \tag{56}$$

7.2.3. $|\hat{\mathcal{N}}_\theta| = 3$ and $|\hat{\mathcal{N}}_\phi| = 1$

The Earth vector in body frame $\hat{r}^{\mathrm{B}}$ is easily accessed solving the linear system (51). The remaining equation of (51) is

$$n_{i_1}^\top \hat{s}^{\mathrm{B}} = \cos(\hat{\phi}_i)\|s\|\,. \tag{57}$$

The indexes $i_2, i_3 \in \{1,\dots,6\}$ can be chosen such that $N = [n_{i_1}\ n_{i_2}\ n_{i_3}]$ is an orthonormal matrix. Then, Equation (48) yields

$$\|s\|^2 = \|N^\top \hat{s}^{\mathrm{B}}\|^2 = (n_{i_1}^\top \hat{s}^{\mathrm{B}})^2 + (n_{i_2}^\top \hat{s}^{\mathrm{B}})^2 + (n_{i_3}^\top \hat{s}^{\mathrm{B}})^2\,.$$

Substituting $n_{i_3}^\top \hat{s}^{\mathrm{B}}$ using Equation (55) leads to

$$\begin{aligned} 0 &= (n_{i_1}^\top \hat{s}^{\mathrm{B}})^2 + (n_{i_2}^\top \hat{s}^{\mathrm{B}})^2 - \|s\|^2 \\ &\quad + \Big(-\frac{\hat{r}^{\mathrm{B}\top} n_{i_2}}{\hat{r}^{\mathrm{B}\top} n_{i_3}} n_{i_2}^\top \hat{s}^{\mathrm{B}} + \frac{r^\top s - \hat{r}^{\mathrm{B}\top} n_{i_1} n_{i_1}^\top \hat{s}^{\mathrm{B}}}{\hat{r}^{\mathrm{B}\top} n_{i_3}}\Big)^2 \\ &= \Big(1 + \Big(\frac{\hat{r}^{\mathrm{B}\top} n_{i_2}}{\hat{r}^{\mathrm{B}\top} n_{i_3}}\Big)^2\Big)(n_{i_2}^\top \hat{s}^{\mathrm{B}})^2 \\ &\quad - 2\frac{\hat{r}^{\mathrm{B}\top} n_{i_2}}{\hat{r}^{\mathrm{B}\top} n_{i_3}} \frac{r^\top s - \hat{r}^{\mathrm{B}\top} n_{i_1} n_{i_1}^\top \hat{s}^{\mathrm{B}}}{\hat{r}^{\mathrm{B}\top} n_{i_3}} n_{i_2}^\top \hat{s}^{\mathrm{B}} \\ &\quad + \Big(\frac{r^\top s - \hat{r}^{\mathrm{B}\top} n_{i_1} n_{i_1}^\top \hat{s}^{\mathrm{B}}}{\hat{r}^{\mathrm{B}\top} n_{i_3}}\Big)^2 + (n_{i_1}^\top \hat{s}^{\mathrm{B}})^2 - \|s\|^2\,. \end{aligned} \tag{58}$$

This is a quadratic equation in $n_{i_2}^\top \hat{s}^{\mathrm{B}}$ which yields two estimations $n_{i_2}^\top \hat{s}^{\mathrm{B},k}$ for $k \in \{1,2\}$. With (55), (57) and (56) two valid estimations $\hat{s}^{\mathrm{B},k}$ can be found for $k \in \{1,2\}$. It may be possible to rule out one of the two estimations by checking Condition (50a). However, this depends on s and the real attitude q.

7.2.4. $|\hat{\mathcal{N}}_\theta| = 2$ and $|\hat{\mathcal{N}}_\phi| = 2$

The system of equations has the form

$$n_{i_1}^\top \hat{s}^{\mathrm{B}} = \cos(\hat{\phi}_i)\|s\| \qquad n_{i_2}^\top \hat{s}^{\mathrm{B}} = \cos(\hat{\phi}_j)\|s\| \tag{59a}$$
$$n_{j_1}^\top \hat{r}^{\mathrm{B}} = -\cos(\hat{\theta}_i)\|r\| \qquad n_{j_2}^\top \hat{r}^{\mathrm{B}} = -\cos(\hat{\theta}_j)\|r\|\,. \tag{59b}$$

Then, $i_3, j_3 \in \{1,\dots,6\}$ can be chosen such that $N_\phi = [n_{i_1}\ n_{i_2}\ n_{i_3}]$ and $N_\phi = [n_{j_1}\ n_{j_2}\ n_{j_3}]$ are orthonormal matrices. Using the normalisation (48) with Equation (59) leads to the system of equations

$$(n_{i_3}^\top \hat{s}^{\mathrm{B}})^2 = \|s\|^2 - (n_{i_1}^\top \hat{s}^{\mathrm{B}})^2 - (n_{i_2}^\top \hat{s}^{\mathrm{B}})^2 \tag{60a}$$
$$(n_{j_3}^\top \hat{r}^{\mathrm{B}})^2 = \|r\|^2 - (n_{j_1}^\top \hat{r}^{\mathrm{B}})^2 - (n_{j_2}^\top \hat{r}^{\mathrm{B}})^2 \,. \tag{60b}$$

Due to the quadratic nature of (60) there are two solutions $n_{i_3}^\top \hat{s}^{\mathrm{B},k}$ and $n_{i_3}^\top \hat{r}^{\mathrm{B},k}$ for $k \in \{1,2\}$. Combining these with (59) leads to four possible solutions $(\hat{s}^{\mathrm{B},k}, \hat{r}^{\mathrm{B},l})$

$$\hat{s}^{\mathrm{B},k} = N_\phi^{-1}\|s\| \begin{pmatrix} \cos(\hat{\phi}_i) \\ \cos(\hat{\phi}_j) \\ (-1)^k\sqrt{1-\cos(\hat{\phi}_i)^2-\cos(\hat{\phi}_j)^2} \end{pmatrix} \tag{61a}$$

$$\hat{r}^{\mathrm{B},l} = N_\theta^{-1}\|r\| \begin{pmatrix} -\cos(\hat{\theta}_i) \\ -\cos(\hat{\theta}_j) \\ (-1)^{l+1}\sqrt{1-\cos(\hat{\theta}_i)^2-\cos(\hat{\theta}_j)^2} \end{pmatrix} \tag{61b}$$

for $k, l \in \{1,2\}$. Verifying Equation (49) shows that only two of these four solutions are valid. Finally, the Conditions (50) may rule out an additional solution dependent on q, s and r.

7.2.5. $|\hat{\mathcal{N}}_\theta| = 2$ and $|\hat{\mathcal{N}}_\phi| = 1$

In this case the solution is obtained in the same manner as 7.2.3 but for two possible estimations of $\hat{r}^{\mathrm{B},l}$ obtained by (60b) for $l \in \{1,2\}$. With the potential two solutions $\hat{s}^{\mathrm{B},k}$ obtained as in Section 7.2.3 this leads to potentially four solutions which need to fulfil the Conditions (50).

7.2.6. $|\hat{\mathcal{N}}_\theta| \leq 1$ and $|\hat{\mathcal{N}}_\phi| \leq 1$

For the case of $|\hat{\mathcal{N}}_\theta| = 1$ and $|\hat{\mathcal{N}}_\phi| = 1$ system of equations has the form

$$\hat{s}^{\mathrm{B}} n_{i_1} = \cos(\hat{\phi}_{i_1})\|s\| \qquad \hat{r}^{\mathrm{B}} n_{j_1} = \cos(\hat{\theta}_{j_1})\|r\| \,. \tag{62}$$

By choosing $n_{i_2}^\top \hat{s}^{\mathrm{B}} \in [0, \|r\|^2 - (\hat{r}^{\mathrm{B}} n_{i_1})^2]$ the task is reduced to the same one as in Section 7.2.5. This makes clear that the resulting number of solutions is not finite any more. The same reasoning can be applied for even fewer sensors. Thus, it is sensible in this case to make use of higher order temperature derivatives as e.g. illustrated in Posielek and Reger (2022) or rely on the integration of the angular velocity instead if the initial attitude is sufficiently accurate.

The results are summarised in the following proposition.

Proposition 7.1 *In case of a sensor outage such that at least one functioning sensor is sunlit and at least two are influenced by Earth irradiation or vice versa, i.e. for all attitudes $q \in \mathbb{S}_3$ holds*

$$(|\mathcal{N}_\phi(q)| \geq 1 \,\wedge\, |\mathcal{N}_\theta(q)| \geq 2) \,\vee\, (|\mathcal{N}_\phi(q)| \geq 2 \,\wedge\, |\mathcal{N}_\theta(q)| \geq 1)$$

then the real attitude is contained in a set of at most four possible attitudes $\hat{q}^k$. An error of the possible attitudes can be defined via

$$e_k = \sum_{n_i \in N_\phi^{\mathrm{ld}}} \left|\cos(\hat{\phi}_i) - \max\left(\frac{s^\top}{\|s\|}A(q^k)^\top n_i, 0\right)\right| + \sum_{n_i \in N_\theta^{\mathrm{ld}}} \left|\cos(\hat{\theta}_i) - \max\left(\frac{r^\top}{\|r\|}A(q^k)^\top n_i, \cos(\theta_{\mathrm{crit}})\right)\right| . \tag{63}$$

which is identical to zero for the real attitude.

Proof: Using the algorithm proposed in 5 with the body vector estimations proposed in 7.2.1 to 7.2.5 allows to obtain the possible attitudes. The Equations (50) are incorporated into (63) which is identical to zero for the correct attitude but not necessarily for the other possible attitudes. □

Table 1: Number of possible attitudes.

$\lvert\hat{\mathcal{N}}_\theta(q)\rvert$	$\lvert\hat{\mathcal{N}}_\phi(q)\rvert$	Attitudes
3	≥ 2	1
3	1	1-2
2	2	1-2
2	1	1-4
≤ 1	≤ 1	∞

An overview of the possible solutions dependent on the number of normals can be seen in Table 1. Note that the proposed algorithms can be easily extended for the case of a spacecraft in solar eclipse with the estimation of only the earth vector without the possibility of estimating the vector to sun.

Validation on real data of the proposed algorithms can be found in the next section.

Table 2: Sun position, initial spacecraft position and spacecraft velocity.

Variable	Value
s	$\begin{bmatrix}1.4779 & 0.1984 & 0.0860\end{bmatrix}^\top \cdot 10^{11}\,\mathrm{m}$
r_0	$\begin{bmatrix}-1.9265 & -1.8703 & -6.2987\end{bmatrix}^\top \cdot 10^{6}\,\mathrm{m}$
v_0	$\begin{bmatrix}-4.79 & -5.11 & 2.98\end{bmatrix}^\top \cdot 10^{3}\,\mathrm{m\,s^{-1}}$

8. Observer Validation on Real Mission Data

In this section the observer designs from Section 5 and 7 are employed on data acquired from a real mission. First, the data obtained is described in detail, then the parameter identification is discussed and finally the reconstruction capabilities of the observer are validated.

8.1. Mission Data Sets

The reference mission considered is the Gravity Recovery and Climate Experiment (GRACE) Mazanek (2000); Kirschner et al. (2001); Larson et al. (2007); Bertiger et al. (2002). The mission launched in March 2002 consists of

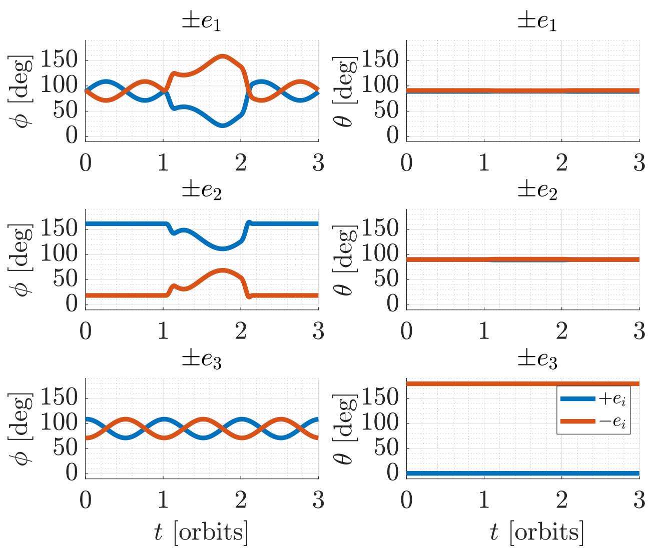

Figure 6: Angles between the sensor normals of the spacecraft and Sun and Earth.

two twin satellites which took detailed measurements to improve the model of the Earth's gravity field .

The data sets considered consist of the time t when a measurement is obtained, the corresponding position and velocity of the spacecraft r and v, the current attitude of the spacecraft q and twelve temperature measurements T. Relevant parts of the received data are presented to provide an overview of the interesting dynamics.

The data considered is from 2014/04/11 00:00:00 UT with a sample rate of 1 s. The corresponding orbit is a low Earth orbit as it has a semi-major axis of approximately 6800 km, i.e. an altitude of about 450 km. This leads to a period of the orbit T^{Orbit} of approximately 92.98 minutes. Further, the orbit is almost circular with an eccentricity of 0.003 and it is a polar orbit with an inclination of about 89 degrees. For the longitude of the ascending node (LTAN) holds $\Omega = 126.39°$. During the considered time, the spacecraft orbit is never in solar eclipse. The initial positions and velocities of the spacecraft and the position of the Sun in ECI can be found in Table 2.

The attitude of the spacecraft is defined by the mode the spacecraft is in. In science mode the attitude is described by the Orbit frame Markley and Crassidis (2014), i.e. the z-axis is pointing along the nadir vector, the y-axis is pointing along the negative orbit normal in the direction opposite to the spacecraft's orbital angular velocity. An additional pitch of -0.92 degrees is due to the twin satellites pointing towards each other. The x-axis completes the right-handed triad. The second mode considered is the slew mode, in which the spacecraft performs a slew manoeuvre over the course of 107.2 minutes (≈ 1.15 orbits). During the slew manoeuvre the spacecraft rotates 90 degrees around its body z-axis and remains in the new attitude for 78.8 minutes and then rotates back -90 degrees. The attitude for the time series is illustrated by the means of their angles to Sun and Earth in Figure 6. The time is normalised such that the x-axis displays the time passed in orbits, i.e. $t^{\text{Orbit}} = \frac{t-t_0}{T^{\text{Orbit}}}$ where t_0 is chosen such that the slew manoeuvre starts exactly after the first orbit. Before and after the slew mode the spacecraft is in science mode.

The evolution of the angles between the individual normals and Sun and Earth vector are shown in Figure 6. Every plot displays two angles for normals in opposing unit directions. Note that there is always a simple connection between two angles for normals pointing into opposing direction. One results from the other by subtracting the angle from 180 degrees as in (36). The left column displays the sun angles ϕ, the right column displays the earth angles θ. In the first plot in the left column the angle to the Sun for the normal vector pointing in and oppose the velocity direction can be seen. It can be seen that during science mode, both angles can be approximately defined by a sinus function with a mean of 90 degrees and an amplitude of approximately 20 degrees. Their phase is shifted with exactly 180 degrees. The second plot in the left column shows the angles for the two normal vectors pointing perpendicular to the orbit. The angles are constant during science mode over the course of an orbit, due to the position of the Sun varying very slowly in this time frame. One angle is about 160 degrees while the other one is approximately 30 degrees. Latter side is commonly referred to as the side pointing towards the Sun. The third plot in the left column shows the angles to the Sun of the zenith and nadir pointing side. These have a similar behaviour as the sides pointing into velocity direction. The solar angles become interesting for the normals in and oppose to velocity direction during the slew manoeuvre. The side along e_1 makes a quick motion towards the Sun, then points gradually away and then back to it until the angle reaches its minimum. This behaviour is mirrored by the side pointing into $-e_1$ direction. The sides pointing perpendicular to the orbit endure a qualitatively similar motion. The sides pointing zenith and nadir are not influenced by the motion as the rotation is around the z-axis.

In the second column the angles between the vector to Earth and each surface normal can be seen. These are all constant because the spacecraft is controlled to follow the orbit frame with its body z-axis always pointing in nadir direction. Consequently, the angles of the sides pointing nadir $+e_3$ and zenith $-e_3$ have approximately 0 and 180 degrees, respectively. The angles of the other four sides are all about 90 degrees. Note that small deviations to these values can be seen because of the additional -0.92 degrees pitch. These angles do not change during the slew manoeuvre due to the rotation being around the z-axis.

Figure 7 shows the twelve temperature measurements over the course of three orbits. Each column consist of three plots, each containing two temperature measurements with opposing normals. The left column shows the temperatures for the black sensors and the right column shows the temperatures for the silver sensors. Three or-

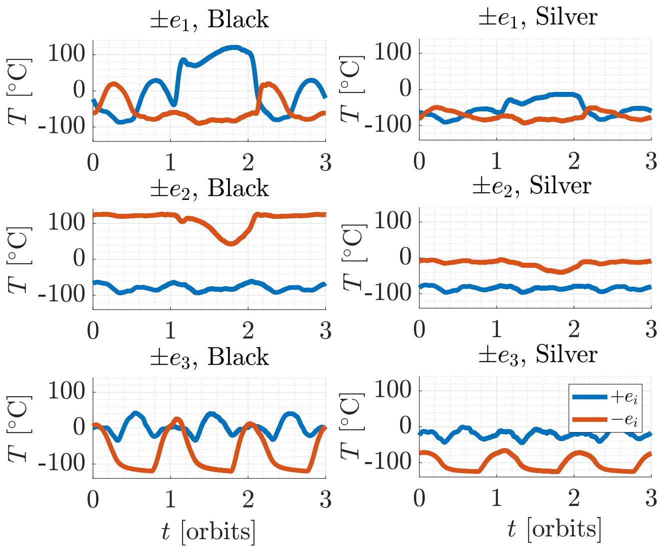

Figure 7: Temperature measurements T_i.

bits are displayed and it can be seen that the measurements are almost periodic with a period of one orbit. The top plot in the left column shows the temperature of the black sensor pointing in and oppose to the velocity direction of the spacecraft. Both sensors show similar qualitative behaviour in science mode. Under the influence of solar irradiation the temperature rises with the solar angle to its maximum of around 20 degrees Celsius and then drops back to approximately -80 degrees Celsius when no solar irradiations is acting any more. This behaviour results mostly from the sinusoidal evolution of the angles. The middle plot shows the temperature of the black sensor pointing towards and oppose the orbit normal. The temperature of the sensor with the normal pointing toward the Sun is almost constant during science mode. This suggests that the influence of the solar irradiation is dominant on this side. For the opposite side, no solar irradiation is acting. Here the temperature evolution is dominated by the albedo and the infrared irradiation. Oscillations occur because of varying albedo and infrared irradiation factors. These depend on the current cloud coverage and the terrain the spacecraft passes. The bottom plot on the left column shows the evolution of the measured temperature from the sensors pointing towards zenith and nadir. For the nadir pointing sensor e_3 the influence of solar irradiation can clearly be identified. During these times the temperature rises significantly. For the remaining parts, the evolution is dominated by the influence of infrared as well as albedo irradiation. This leads to a highly time variant temperature signal due to the changing surface of the Earth. A more distinct temperature evolution can be observed by the sensor pointing towards zenith $-e_3$. Here, only solar irradiation is acting and the sinusoidal influence of the solar angle can be seen. The temperature evolutions for the silver sensors are qualitatively almost identical. The main difference lies in the amplitude of the temperatures as the influence of the solar irradiation on the temperature is diminished.

After orbit one, the slew manoeuvre starts. Here, the temperature evolution follows roughly the evolution of the solar angles ϕ during the slew manoeuvre. Afterwards, the temperature returns to its periodic behaviour in science mode.

This data is used in the upcoming sections to fit the proposed model on the science mode data up to the first orbit and validate the results on the slew mode starting after the first orbit.

8.2. Parameter Identification

In this section, the attitude q between orbit zero and one is considered to be known and use it with the measured temperatures and position to identify the other parameters depending on the spacecraft and its thermal topology. More precisely, the optimal numerical values of the five parameters C, α_s, ε_e, A_s and Q^d is determined based on the temperature data for each sensor.

In order to reduce the amount of parameters to be estimated, it is important to determine which parameters are redundant in the system dynamics sense. It can be readily verified that the parameter tupel $(C, \alpha_\mathrm{s}, \varepsilon_\mathrm{e}, A_\mathrm{s}, Q^\mathrm{d})$ and $(abC, a\alpha_\mathrm{s}, a\varepsilon_\mathrm{e}, bA_\mathrm{s}, abQ^\mathrm{d})$ yield the same dynamics (1) for $a, b \in \mathbb{R} \setminus \{0\}$. Consequently, two of these parameters can be arbitrarily chosen for the estimation process. The parameters A_s and ε_e are chosen to allow an easier comparison of the dynamics and the thermal properties. The values are set to be $A_\mathrm{s} = 1$ and $\varepsilon_\mathrm{e} = 0.8$.

In order to allow an unbiased fit, the measured trajectories T_i are divided into the first orbit in science mode which is used for fitting and the remaining time that is used for validation purposes.

Then the optimisation problem can be divided into 12 different optimisation problems, each of the form

$$\min_{c_i} \quad \int_0^{t_\mathrm{end}} |T_i(t) - \hat{T}_i(t)| \mathrm{d}t \tag{64a}$$

$$\text{s. t.} \quad \dot{\hat{T}}_i = f_i(\hat{T}_i, q, r, n_i, c_i) \tag{64b}$$

$$(\alpha_{\mathrm{s},i}, C_i, Q_i^\mathrm{d}) \subset [0,1] \times \mathbb{R}^+ \times \mathbb{R}_0^+ \tag{64c}$$

for $i \in \{1, \ldots, 12\}$. Every problem has 3 optimisation parameters (64c) and only a single dynamic equation (64b). The presented optimisation problem could be adapted vowing in for example some additional constraints such as e.g. $\alpha_{\mathrm{s},i} = \alpha_{\mathrm{s},j}$ for $i \in \{1, \ldots, 6\}$ as these sensors have the same coatings. However, the proposed optimisation problem was chosen to be used as it is the simplest to solve and yields models that give the best temperature estimation based on the proposed optimisation problems.

In order to solve the optimisation problem (64), the software environment MOPS (Multi-Objective Parameter Synthesis), an optimisation tool of the Institute of System Dynamics and Control of the German Aerospace Center presented in Joos (2002), is used. In Table 3 the optimal

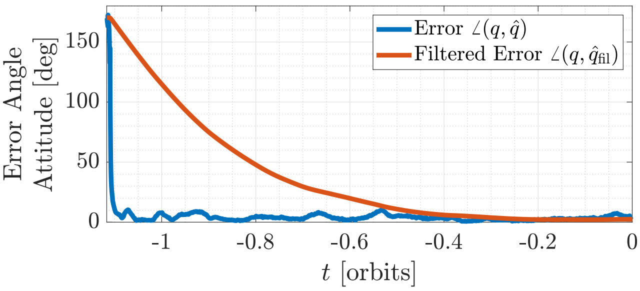

Figure 8: Evolution of the error angle of the attitude in the transient phase.

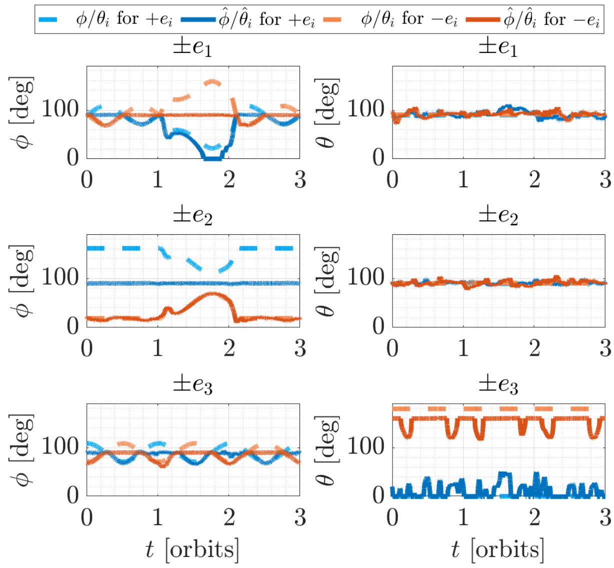

Figure 9: Estimated angles $\hat{\phi}$ and $\hat{\theta}$ compared with the real angles ϕ and θ for the normal $n = \pm e_i$.

parameters can be seen for a fit on the science mode data, i.e. $t_{\mathrm{end}} = 1$.

To give a compact evaluation of all the fits the coefficient of determination R^2 is used. It is defined as

$$R^2 = 1 - \frac{\sqrt{\sum_{k=1}^{N} |y_k - \hat{y}_k|^2}}{\sqrt{\sum_{k=1}^{N} |y_k - \hat{y}^{\mathrm{av}}|^2}}$$

with the measurement values $y_k = T_i$, the values obtained from the model $\hat{y}_k = \hat{T}_i$ with the average value $\hat{y}^{\mathrm{av}} = \frac{1}{N}\sum_{k=1}^{N} \hat{T}_i(t_k)$ for the measurement times $(t_k)_{k\in\mathbb{N}} = (1, \ldots, N)$ and the sensors $i \in \{1, \ldots, 12\}$. Table 4 shows the R^2-values of the twelve configurations. It can be seen that all values are very close to one which suggests that the fitted model is appropriate. Additional discussion and verification of these parameters can be found in Posielek (2022).

8.3. Observer Validation

In this section the proposed observer from Section 5 are used to estimate the attitude q solely based on the GRACE measurements discussed in Section 8.1. Additionally, a sensor outage is simulated and the algorithms of Section 7 are used to validate the possibility to estimate the attitude despite the outage of a temperature sensor.

8.3.1. Nominal Operation

In this section the nominal operation mode is considered with all sensors working and providing the real measurement data shown in Section 8.1. The observer proposed in the Section 5 is shown with the additional nonlinear filter discussed in Section 6 to smooth the estimation. For the position r the measurements obtained from the data sets are directly used. The angular velocity measurements $\hat{\omega}$ were unfortunately unavailable and are thus generated using

$$\hat{\omega} = (I_3 + S)\omega + \beta_\omega + \eta_\omega$$

with the matrix $S = \left(s_{S,1}^\top \; s_{S,2}^\top \; s_{S,3}^\top\right)$ with $s_1^\top = [15\;10\;15] \cdot 10^{-4}$, $s_2^\top = [15\;\;10\;\;15] \cdot 10^{-4}$, $s_3^\top = [10\;\;15\;\;15] \cdot 10^{-4}$ incorporating scale and misalignment factors, the bias $\beta_\omega = [0.48\;0.48\;0.48] \cdot 10^{-6}\,\mathrm{rad\,s^{-1}}$ and the Gaussian white noise η_ω with the standard deviation $\sqrt{10} \cdot 10^{-7}\,\mathrm{rad}/\sqrt{\mathrm{s}}$ Markley and Crassidis (2014). The time t with respect to the orbit period as in Section 8.1 is used. Thus, the simulation starts at a normalised time of around -1.1 orbits with the initial attitude $q_0 = [-0.88\;0.44\;0.15\;0.085]^\top$ and the initial guess $\hat{q}_0 = [0\;\;0\;\;0\;\;1]^\top$ which corresponds to an initial error of around 170 degrees. The gains of the linear differentiator $a_0 = 40.33$, $a_1 = 41.33$ and $\varepsilon = 50.244$ are obtained by an optimisation which minimises the error $\int_0^1 \angle(s_{\mathrm{B}}, \hat{s}_{\mathrm{B}}(t)) + \angle(r_{\mathrm{B}}(t), \hat{r}_{\mathrm{B}}(t))\mathrm{d}t^{\mathrm{Orbit}}$ where the integration time is in orbits with $t = t^{\mathrm{Orbit}} T^{\mathrm{Orbit}} + t_0$. The filter gain $k = 0.0017$ is obtained minimising the angle error $\int_0^1 \angle(q(t), \hat{q}_{\mathrm{filt}}(t))\mathrm{d}t^{\mathrm{Orbit}}$.The small value of k is sensible as it allows a slow convergence of the attitude for high initial errors a the benefit of better filtering qualities. The slow convergence is also justified by the slow dynamics that the spacecraft is considered in this mission. Note that the optimisation is only carried out in the first orbit (in SM) in order to allow an evaluation in slew mode.

The observer proposed in Section 5 guarantees the convergence of the estimates to the real attitude when no measurements or model errors are present. An estimation including these errors leads only to the convergence to a neighbourhood of zero instead of exact zero. The period until the solution reaches this neighbourhood is referred to as the transient phase. The error of the estimated attitude $\hat{q}$ and the filtered attitude $\hat{q}^{\mathrm{filt}}$ is displayed Figure 8. Without the additional attitude filter the convergence of $\hat{q}$ depends solely on the convergence of the differentiator which is within about 0.01 orbit. With the additional filter the convergence time rises up to approximately 1 orbit. This is a sufficient convergence time for the herein considered initial values and time frame. Faster convergence can

Table 3: Fitted parameters, $i \in \{1, \dots 12\}$

n_i	e_1	$-e_1$	e_2	$-e_2$	e_3	$-e_3$	e_1	$-e_1$	e_2	$-e_2$	e_3	$-e_3$
$\alpha_{\mathrm{s},i}$	0.70	0.57	0.53	0.81	0.50	0.57	0.11	0.13	0.06/0.12	0.11	0.14	0.13
C_i [$\mathrm{K\,s^{-1}}$]	570	392	361	443	495	398	451	484	334	636	463	340
Q_i^{d} [W]	15.57	12.73	8.37	0	24.42	26.10	12.92	11.64	6.62	29.19	3.03	23.24

Table 4: R^2 values.

n_i	e_1	$-e_1$	e_2	$-e_2$	e_3	$-e_3$
R^2 for $n_1 - n_6$	0.992	0.986	0.918	0.996	0.916	0.991
R^2 for $n_7 - n_{12}$	0.979	0.964	0.848	0.970	0.913	0.983

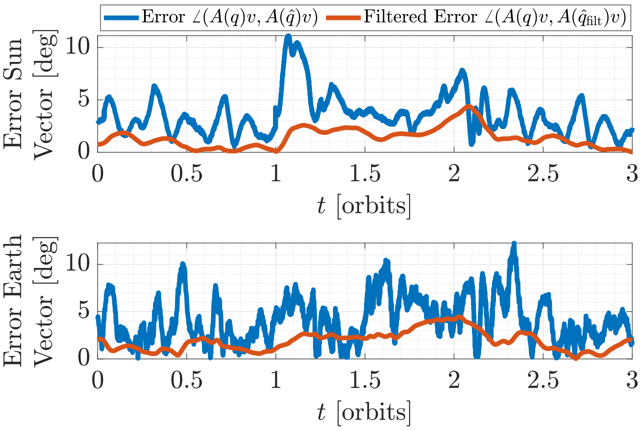

Figure 10: Angle error between the estimated vector and the real vectors $v \in \{s, r\}$.

also be achieved by adjusting the filter gain at the cost of higher stationary errors.

The stationary behaviour to be between orbit 0 and 3 is considered. Figure 9 shows all twelve estimated angles $\hat{\phi}$ and $\hat{\theta}$ over the number of orbits. The style of the display is the same as in Figure 6 where only the corrected angles values are shown. The dashed line represents the real angles and the solid line displays the estimated angles. The top plot in the left column shows the estimates of the solar angle for the sensors pointing in and oppose the velocity direction. During the first orbit in science mode the angles below 90 degrees are estimated with good accuracy. As expected, angles over 90 degrees are estimated to be 90 degrees by the algorithm. During the slew manoeuvre the estimation error becomes more visible as the solar irradiation estimate appears to be higher than it actually is. This suggests that lower values in the model for the parameter α_{s} may improve this estimation. The middle plot in the left column displays the angle of the sensors perpendicular to the orbit plane. It can be seen that the estimates are extremely accurate even during the slew manoeuvre. The bottom plot in the left column shows the estimates for the nadir and zenith pointing sensors. Here the estimation shows some small errors during the science mode as well as the slew mode. In particular, the large error during the start of the slew manoeuvre is due to some dynamics that have not been incorporated in the model. For the second column the top and middle plots show the angle to Earth of the sensors pointing in direction of the velocity and perpendicular to the orbit plane. These errors are higher than the ones from the solar angle but they appear to oscillate around the correct mean value. The bottom plot in the second column shows the estimates for the angles to $\pm e_3$. The normal $-e_3$ is pointing towards zenith and can therefore not be correctly estimated and leads instead mostly to an estimation of the maximal angle. It is very interesting to note that there are multiple points when the error of the estimated angle θ_5 becomes very large. This is most likely to internal heat flows which are not modelled. The normal $+e_3$ is pointing towards nadir, the estimation shows some significant errors for this normal as the time variance of the infrared and albedo irradiation is only roughly incorporated in the model.

Figure 10 shows the error angle of estimated Sun and Earth vector and the error angle of the angle estimated resulting from the final filtered attitude $\hat{q}^{\mathrm{filt}}$. Table 5 shows the mean and the standard deviation of these error angles. From Figure 10 it can be seen that in science mode the unfiltered error angle between the Sun vector and its estimate is of low dynamics in comparison to the error angle of the Earth vector. Additionally, during science mode the solar vector is more accurately estimated than the Earth vector. Remember that the model was fitted to the data during science mode which is why it is expected to have better results in science mode than in slew mode. Indeed, during slew mode the estimate of both vectors becomes less accurate. For the solar vector, a significant spike occurs at the start of the manoeuvre as discussed due to the high error in the estimate of the ϕ angle in e_1 direction. The Earth vector estimate admits larger errors during the second phase of the orbit. The filtered error admits overall smaller errors with slower dynamics.

Figure 11 and Table 5 show the error of the estimated attitude $\hat{q}$ and the filtered attitude $\hat{q}^{\mathrm{filt}}$. It can be seen that as expected the filtered attitude damps the oscillation while giving overall more accurate estimations despite the errors in the measurements of the angular velocity. For both estimations it can be seen that the results are better during the science mode than during the slew mode. This can be mainly ascribed to the fact that the data from the science mode was used to fit the parameters in Section 8.2. However, the results in slew mode show that the resulting model yields results in the desired accuracy. It can be seen that for both estimations the fluctuation of the error is comparatively high. There are multiple potential reasons for this. First and foremost, unmodelled thermal dynamics, mainly in the form of internal heat flows, may lead

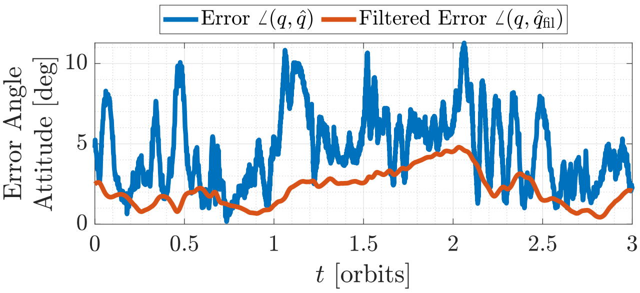

Figure 11: Error between real and estimated attitude.

Table 5: Mean and Standard deviation of the error angles of the estimated vectors and attitude. The science mode (SM) denotes the time frame until the first orbit and the slew mode (Slew) denotes the time frame from the first orbit when the slew manoeuvre starts to the end of the slew manoeuvre. Total denotes the mean and the standard deviation for the combined time frame.

Error Angle	Mean [deg]			Standard Deviation [deg]		
	SM	Slew	Total	SM	Slew	Total
$\angle(s^{\text{B}},\hat{s}^{\text{B}})$	2.8	4.86	3.84	1.28	2.20	2.07
$\angle(r^{\text{B}},\hat{r}^{\text{B}})$	3.30	4.86	4.08	2.09	2.18	2.28
$\angle(q,\hat{q})$	3.47	5.97	4.72	2.09	1.76	2.30
$\angle(q,\hat{q}_{\text{filt}})$	1.43	3.03	2.23	0.51	0.81	1.04

to such high variations. If more knowledge about these unknown heat flows is available, it is possible to incorporate them into the model design and reduce the variations. Additionally, the parameter identifiction in Section 8.2 is optimised to minimise the temperature error for the individual sensors. A different optimisation criteria could be chosen which can lead to a smaller fluctuation. All in all, the mean of the total error is about five degrees for the attitude estimation and even about two degrees for the filtered attitude as can be seen in Table 5 which makes the method a viable option for attitude estimation.

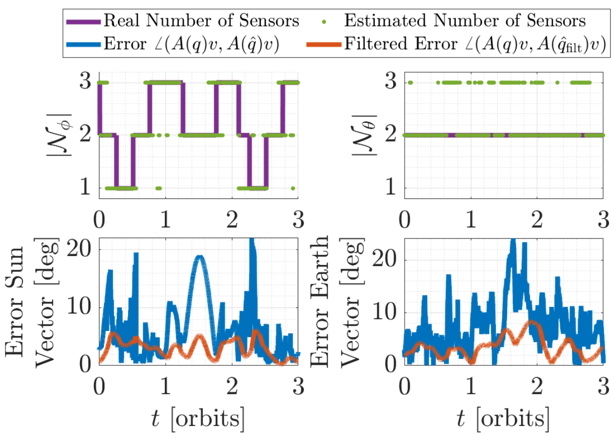

Figure 12: Real and estimated number of sensors under the influence of solar and Earth irradiation. Error between the real and estimated Sun and Earth vector, $v \in \{r, s\}$.

8.3.2. Sensor Failure

In this section, at 0 orbits the outage of the temperature sensors is considered. These are pointing along e_1, $-e_2$ and $-e_3$ direction, i.e. $\bar{N}^{\text{con}} = \{-e_1, e_2, e_3\} = \{n_2, n_4, n_6\}$. The differentiator and filter with the same gains as in the previous Section 8.3.1 and the same algorithms proposed in Section 7 are used.

The main difficulty lies within the estimation of the set $\hat{\mathcal{N}}_\phi(q), \hat{\mathcal{N}}_\theta(q)$. Due to $\hat{\phi}_i$ and $\hat{\theta}_i$ being subject to model and measurements errors, the definition (47) may lead to incorrect estimates and the usage of sensors for the reconstruction that may carry false information. There are different ways to improve the estimation of $\hat{\mathcal{N}}_\phi(q)$. Multiple pairs of sets $(\hat{\mathcal{N}}^1_\phi(q), \hat{\mathcal{N}}^1_\theta(q))$, ..., $(\hat{\mathcal{N}}^{n_{\text{lit},\phi}}_\phi(q), \hat{\mathcal{N}}^{n_{\text{lit},\phi}}_\theta(q))$ are defined and the reconstruction obtaining the estimated attitudes $\hat{q}^1 \ldots \hat{q}^{n_{\text{lit},\phi}}$ are carried out where $n_{\text{lit},\phi} \in \mathbb{N}$ is the number of considered estimates. The final estimate is based on the smallest error (63), i.e. $\hat{q} = \hat{q}^{k_{\min}}$ where $k_{\min} = \text{argmin}_k\, e(k)$ and e is considered as the function which maps k to the error e_k defined in (63). The sets $\hat{\mathcal{N}}^i_\phi(q)$ are obtained as in (47a) with the augmentation that for uncertain angle estimations, two sets $\hat{\mathcal{N}}^i_\phi(q)$, $\hat{\mathcal{N}}^j_\phi(q)$ are defined where one incorporates the corresponding normal while the other does not. An angle estimation is defined to be uncertain if $\hat{\phi}_i > \frac{\pi}{2} - \phi^{\text{thr}}$ where $\phi^{\text{thr}} \in \mathbb{R}$ is a designed threshold. The same is carried out for $\hat{\mathcal{N}}^j_\theta(q)$. All combinations of these two sets $\hat{\mathcal{N}}^i_\phi(q), \hat{\mathcal{N}}^j_\theta(q)$ lead to the considered pairs of sets. As the thresholds $\phi^{\text{thr}} = 0.26$ and $\theta^{\text{thr}} = 0.87$ based on the estimates in Science Mode displayed in Figure 9 are chosen.

The transient phase of the estimation is identical to the one in Figure 8 because the outage occurs at 0 orbits. The estimates of the stationary phase can be seen in Figure 12. The top row shows the real and estimated number of sensors under the influence of solar and Earth irradiation. It can be seen that despite the improved algorithm the estimation is not always correct for the number of sensors that are sunlit. The errors become more frequent at the transition points when the state of a sensor changes between sunlit and not sunlit. The number of sensors under Earth irradiation is constant with a value of two over the considered time. The estimation is correct most of the time but at some instances the zenith pointing sensor is considered in the estimation of the Earth vector. For the error of the Earth and Sun vector estimates it can be seen that the error is high when the estimated number of sensors under Sun and Earth irradiation is not correct. Higher errors compared to Figure 10 can be observed during the slew manoeuvre which is mainly because the information from the nadir pointing sensor is missing. Overall, as can be seen in Table 6, the mean error is about three degrees higher than in the nominal case for both Sun as well as Earth vector estimation.

Figure 13 shows the error angle of the estimated attitude $\hat{q}$ and the final filtered attitude $\hat{q}^{\text{filt}}$. Their evolution is qualitatively similar to the errors displayed in Figure 11.

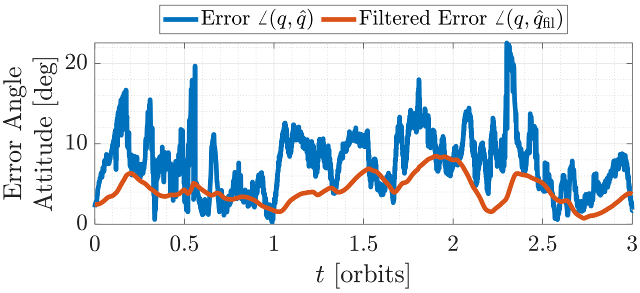

Figure 13: Error between real and estimated attitude.

Table 6: Error angles as in Table 5 for the considered sensor outage

Error Angle	Mean [deg] SM	Slew	Total	Standard Deviation [deg] SM	Slew	Total
$\angle(s^{\text{B}},\hat{s}^{\text{B}})$	4.76	9.39	7.07	3.80	5.18	5.10
$\angle(r^{\text{B}},\hat{r}^{\text{B}})$	4.87	10.71	7.79	2.82	5.10	5.05
$\angle(q,\hat{q})$	6.32	9.00	7.66	3.82	2.70	3.57
$\angle(q,\hat{q}_{\text{filt}})$	3.80	5.24	4.52	1.04	1.88	1.68

However, the mean error is about three degrees higher for the unfiltered attitude and about two degrees higher for the filtered attitude as can be seen in Table 6.

9. Conclusion

Observability of the satellite system with temperature measurements as outputs can be ensured. The measurements are obtained by twelve temperature sensors in cuboid configuration. The underlying algorithm can be very well structured into the different tasks of differentiation, angle estimation, vector estimation and finally attitude estimation. Even in the case of partial sensor outage the capabilities of attitude estimation remain feasible but require more complex algorithms. An evaluation of the attitude estimation algorithm based on real mission data from the GRACE mission showed that the error which is to be expected lies in the range of a few degrees. The proposed algorithm can be augmented adding additional vector measurements such as magnetic field or the gravity measurements. The proposed considerations have shown that it is possible to use temperature sensors for the attitude estimation. This can be used in future mission in different ways such as by fusing the temperature measurements with already existing sensors or as a cheap fall back method.

Acknowledgements

The authors kindly acknowledge the organisation unit Mission Operations (MIB-LEM OP) of the German Aerospace Center for providing the data sets of the GRACE mission. The second author gratefully acknowledges the financial support from European Union Horizon 2020 research and innovation program, Marie Skłodowska-Curie grant agreement No. 824046.

References

Bertiger, W., Bar-Sever, Y., Desai, S., Dunn, C., Haines, B., Kruizinga, G., Kuang, D., Nandi, S., Romans, L., Watkins, M., et al., 2002. GRACE: millimeters and microns in orbit, in: International Technical Meeting of the Satellite Division of The Institute of Navigation, pp. 2022–2029.

Besançon, G., 2007. Nonlinear observers and applications. volume 363. Springer.

Canuto, E., Novara, C., Carlucci, D., Montenegro, C.P., Massotti, L., 2018. Spacecraft Dynamics and Control: The Embedded Model Control Approach. Butterworth-Heinemann.

Gourabi, F.N., Kiani, M., Pourtakdoust, S.H., 2019. Autonomous temperature-based orbit estimation. Aerospace Science and Technology 86, 671–682.

Gourabi, F.N., Kiani, M., Pourtakdoust, S.H., 2020. On-line orbit and albedo estimation using a strong tracking algorithm via satellite surface temperature data. IEEE Transactions on Aerospace and Electronic Systems 57, 1443 – 1454.

Herman, J., Presti, D., Codazzi, A., Belle, C., 2004. Attitude control for GRACE: The first low-flying satellite formation, in: International Symposium on Space Flight Dynamics, pp. 27–33.

Joos, H.D., 2002. A multiobjective optimisation-based software environment for control systems design, in: IEEE International Symposium on Computer Aided Control System Design, pp. 7–14.

Khalil, H.K., 2002. Nonlinear Systems. Third ed., Prentice Hall.

Khaniki, H.B., Karimian, S.M.H., 2014. Determining the heat flux absorbed by satellite surfaces with temperature data. Journal of Mechanical Science and Technology 28, 2393–2398.

Kirschner, M., Montenbruck, O., Bettadpur, S., 2001. Flight dynamics aspects of the GRACE formation flying, in: International Workshop on Satellite Constellations and Formation Flying, pp. 1–8.

Kramer, H.J., 2002. Observation of the Earth and its Environment: Survey of Missions and Sensors. Springer Science & Business Media.

Labibian, A., Alikhani, A., Pourtakdoust, S.H., 2017. Performance of a novel heat based model for spacecraft attitude estimation. Aerospace Science and Technology 70, 317–327.

Labibian, A., Pourtakdoust, S.H., Kiani, M., Sheikhi, A.A., Alikhani, A., 2016. Experimental validation of a novel radiation based model for spacecraft attitude estimation. Sensors and Actuators A: Physical 250, 114–122.

Larson, K.M., Ashby, N., Hackman, C., Bertiger, W., 2007. An assessment of relativistic effects for low earth orbiters: the GRACE satellites. Metrologia 44, 484.

Larson, W.J., Wertz, J.R., 1991. Space Mission Analysis and Design. Springer.

Levant, A., 2003. Quasi-continuous high-order sliding-mode controllers, in: IEEE International Conference on Decision and Control, IEEE. pp. 4605–4610.

Levant, A., Livne, M., Yu, X., 2017. Sliding-mode-based differentiation and its application. IFAC-PapersOnLine 50, 1699–1704.

Levenhagen, J., Duske, N., Wolters, R., 2007. Earth oriented safe mode design based on the EADS Astrium CESS. IFAC Proceedings Volumes 40, 301–304.

Markley, F.L., Crassidis, J.L., 2014. Fundamentals of Spacecraft Attitude Determination and Control. Springer.

Martin, P., Rouchon, P., Rudolph, J., 2004. Invariant tracking. ESAIM: Control, Optimisation and Calculus of Variations 10, 1–13.

Mazanek, D.D., 2000. Aerothermal analysis and design of the gravity recovery and climate experiment (GRACE) spacecraft. NASA.

Meseguer, J., Pérez-Grande, I., Sanz-Andrés, A., 2012. Spacecraft Thermal Control. Woodhead Publishing.

Peyrou-Lauga, R., 2017. Using real earth albedo and earth IR flux for spacecraft thermal analysis, in: International Conference on Environmental Systems, pp. 1–14.

Posielek, T., 2018. A Modelica library for spacecraft thermal analysis, in: The American Modelica Conference, Linköping University Electronic Press. p. 46–55.

Posielek, T., 2022. Observability Studies for Spacecraft Attitude Determination based on Temperature Data. Ph.D. thesis. TU Ilmenau.

Posielek, T., Reger, J., 2021. A novel attitude representation in view of spacecraft attitude reconstruction using temperature data, in: Conference on Modelling, Identification and Control of Nonlinear Systems, pp. 526–531.

Posielek, T., Reger, J., 2022. Attitude reconstruction of a spacecraft from temperature measurements in solar eclipse. analysis and observer design for a not globally observable non-linear system. IEEE Transactions on Control , 1–15Early access.

Sidi, M.J., 1997. Spacecraft dynamics and control: a practical engineering approach. volume 7. Cambridge University Press.

Tayebi, A., 2008. Unit quaternion-based output feedback for the attitude tracking problem. IEEE Transactions on Automatic Control 53, 1516–1520.

Vasiljevic, L.K., Khalil, H.K., 2006. Differentiation with high-gain observers the presence of measurement noise, in: Conference on Decision and Control, IEEE. pp. 4717–4722.